bioRxiv preprint doi: https://doi.org/10.1101/418079; this version posted September 14, 2018. The copyright holder for this preprint (which was not certified by peer review) is the author/funder, who has granted bioRxiv a license to display the preprint in perpetuity. It is made available under aCC-BY-NC-ND 4.0 International license.

The key protein of endosomal mRNP transport binds translational landmark sites of cargo mRNAs

Lilli Olgeiser[1], Carl Haag[1], Susan Boerner[2], Jernej Ule[3], Anke Busch[4], Julian König[4], Michael Feldbrügge[1, $] and Kathi Zarnack[2, $]

$ shared corresponding authorship

[1] Heinrich Heine University Düsseldorf, Institute for Microbiology, Cluster of Excellence on Plant Sciences, 40204 Düsseldorf, Germany
[2] Buchmann Institute for Molecular Life Sciences (BMLS), Goethe University Frankfurt, Max-von-Laue-Str. 15, 60438 Frankfurt am Main, Germany
[3] Department of Molecular Neuroscience, UCL Institute of Neurology, Queen Square, London, WC1N3BG, UK
[4] Institute of Molecular Biology gGmbH, Ackermannweg 4, 55128 Mainz, Germany

Running title: Endosomal mRNP transport

Key words: endosome / fungus / iCLIP / microtubule / RNA-binding protein / RNA transport

Characters: 76,116

[*] **Corresponding authors:**

Dr. Michael Feldbrügge

Institute for Microbiology, Cluster of Excellence on Plant Sciences

Heinrich Heine University Düsseldorf, Universitätsstr. 1, 40225 Düsseldorf, Germany

Phone: +49 (211) 81-15475

feldbrue@hhu.de

Dr. Kathi Zarnack

Buchmann Institute for Molecular Life Sciences (BMLS)

Goethe University Frankfurt, Max-von-Laue-Str. 15, 60438 Frankfurt am Main, Germany

Phone: + 49 (69) 798-42506

kathi.zarnack@bmls.de

bioRxiv preprint doi: https://doi.org/10.1101/418079; this version posted September 14, 2018. The copyright holder for this preprint (which was not certified by peer review) is the author/funder, who has granted bioRxiv a license to display the preprint in perpetuity. It is made available under aCC-BY-NC-ND 4.0 International license.

Abstract

RNA-binding proteins (RBPs) determine spatiotemporal gene expression by mediating active transport and local translation of cargo mRNAs. Here, we cast a transcriptome-wide view on the transported mRNAs and cognate RBP binding sites during endosomal messenger ribonucleoprotein (mRNP) transport in *Ustilago maydis*. Using individual-nucleotide resolution UV crosslinking and immunoprecipitation (iCLIP), we compare the key transport RBP Rrm4 and the newly identified endosomal mRNP component Grp1 that is crucial to coordinate hyphal growth. Both RBPs bind predominantly in the 3´ untranslated region of thousands of shared cargo mRNAs, often in close proximity. Intriguingly, Rrm4 specifically recognises landmark sites of translation, including precise binding of start and stop codons, suggesting an intimate connection of mRNA transport and translation. Towards uncovering the code of recognition, we identify UAUG as specific binding motif of Rrm4 that is bound by its third RRM domain. Altogether, we provide first insights into the positional organisation of co-localising RBPs on individual cargo mRNAs.

bioRxiv preprint doi: https://doi.org/10.1101/418079; this version posted September 14, 2018. The copyright holder for this preprint (which was not certified by peer review) is the author/funder, who has granted bioRxiv a license to display the preprint in perpetuity. It is made available under aCC-BY-NC-ND 4.0 International license.

Introduction

All eukaryotic cells must accurately regulate the expression of proteins in time and space. To this end, many mRNAs accumulate at specific subcellular sites, and their local translation is exactly timed (Eliscovich & Singer, 2017, Holt & Bullock, 2009, Martin & Ephrussi, 2009). mRNA localisation is achieved most commonly by active motor-dependent transport along the cytoskeleton. Functional transport units are messenger ribonucleoprotein complexes (mRNPs), consisting of various RNA-binding proteins (RBPs), accessory proteins and cargo mRNAs. Key factors are RBPs that recognise localisation elements (LEs) within mRNAs. For movement, the RBPs either interact with motors directly or are connected via linker proteins (Holt & Bullock, 2009, Mofatteh & Bullock, 2017).

We discovered co-transport of mRNPs on the cytoplasmic surface of early endosomes as a novel translocation mechanism of cargo mRNAs during hyphal growth in fungi (Baumann, König et al., 2014, Baumann, Pohlmann et al., 2012). These endosomes shuttle along microtubules by the concerted action of plus-end directed kinesin and minus-end directed dynein (Egan, McClintock et al., 2012, Steinberg, 2014). They serve as multipurpose platforms functioning not only during endocytic recycling but also during long-distance transport of whole organelles such as peroxisomes (Guimaraes, Schuster et al., 2015, Haag, Pohlmann et al., 2017, Salogiannis, Egan et al., 2016, Salogiannis & Reck-Peterson, 2016).

Endosomal mRNA transport was uncovered analysing the RBP Rrm4 in the dimorphic phytopathogenic fungus *Ustilago maydis* (Fig. S1A; Haag, Steuten et al., 2015, Vollmeister & Feldbrügge, 2010). Loss of Rrm4 has no effects on the yeast form of the fungus. However, the absence of Rrm4 causes characteristic defects in unipolar growth when switching to the hyphal form: the rate of bipolarly growing hyphae increases and the insertion of basal septa is delayed (Baumann et al., 2014, Becht, Vollmeister et al., 2005). In line with endosomal mRNA transport, Rrm4 binds mRNAs and shuttles on early endosomes along microtubules *in vivo* (Baumann et al., 2012, Becht, König et al., 2006). Using the poly(A)-binding protein

bioRxiv preprint doi: https://doi.org/10.1101/418079; this version posted September 14, 2018. The copyright holder for this preprint (which was not certified by peer review) is the author/funder, who has granted bioRxiv a license to display the preprint in perpetuity. It is made available under aCC-BY-NC-ND 4.0 International license.

Pab1 as an mRNA marker revealed that loss of Rrm4 abolishes this transport, resulting in a gradient of mRNAs declining from the nucleus towards the cell periphery (König, Baumann et al., 2009). Thus, one function of Rrm4 might be the general distribution of mRNAs within hyphae (König et al., 2009).

Initial CLIP experiments with Rrm4 identified target mRNAs encoding chitinase Cts1 and septin Cdc3, among others (Koepke, Kaffarnik et al., 2011, König et al., 2009). The subcellular localisation of both proteins was Rrm4-dependent: Loss of Rrm4 strongly reduced the secretion of the chitinase Cts1. Moreover, shuttling of the Cdc3 protein on early endosomes was abolished, and the gradient of septin filaments at the growth pole of hyphae was no longer formed (Baumann et al., 2014). Since *cdc3* mRNA and its encoded protein are found together with ribosomes on the same shuttling endosomes, we hypothesised that endosome-coupled translation of *cdc3* mRNA during long-distance transport is critical for the efficient formation of septin filaments at the growth pole (Baumann et al., 2014). This was supported by demonstrating that all four septin-encoding mRNAs are present on endosomes and that septin proteins assemble into heteromeric complexes on the cytoplasmic face of endosomes during long-distance transport (Zander, Baumann et al., 2016). Thus, Rrm4-dependent mRNA transport regulates the specific localisation of the corresponding translation products. To understand this complex process at the transcriptome-wide level, we present herein an *in vivo* snapshot of RNA binding sites of endosomal RBPs on cargo mRNAs at single-nucleotide resolution.

Results

Loss of the glycine/glutamine-rich protein Grp1 affects hyphal growth

In order to identify additional protein components involved in endosomal mRNA transport, we performed pilot affinity tag purification using Rrm4 as bait. We identified the potential

bioRxiv preprint doi: https://doi.org/10.1101/418079; this version posted September 14, 2018. The copyright holder for this preprint (which was not certified by peer review) is the author/funder, who has granted bioRxiv a license to display the preprint in perpetuity. It is made available under aCC-BY-NC-ND 4.0 International license.

RBP glycine-rich protein 1 (Grp1; UMAG_02412), which carries an N-terminal RNA recognition motif (RRM) domain followed by a short C-terminal region rich in glycine and glutamine (GQ-rich; Fig. 1A, Fig. S1B). The protein was similar to other small RRM proteins, such as human CIRBP or RBM3 and plant RBG7 (*At*GRP7), all previously described as global stress regulators (Fig. 1A; Kang, Park et al., 2013, Zhu, Buhrer et al., 2016).

For functional analysis, we generated deletion mutants in laboratory strain AB33. In this strain the master transcription factor controlling hyphal growth is under control of an inducible promoter. Thus, hyphal growth can be elicited synchronously by changing the nitrogen source in the medium. The corresponding hyphae grow like wild type by tip expansion at the apical pole, while the nucleus is positioned in the centre and septa are inserted in regular intervals at the basal pole (Fig. S1A; Brachmann, Weinzierl et al., 2001). In the yeast form of AB33, we observed that loss of Grp1 resulted in slower proliferation as well as increased cell size (Fig. S1C-E). At lower temperatures, growth of the *grp1Δ* strain was affected even more strongly and it exhibited an altered colony morphology (Fig. S1F). This was consistent with a potential function in cold stress response, similar to the plant and human orthologues (Kang et al., 2013, Zhu et al., 2016). Furthermore, colony growth of the *grp1Δ* strain was strongly reduced upon treatment with inhibitors of cell wall biosynthesis, such as Calcofluor White (CFW) or Congo Red (CR; Imai, Noda et al., 2005, Ram & Klis, 2006). Hence, loss of Grp1 might cause defects in cell wall formation (Fig. S1G).

Studying hyphal growth revealed that, unlike observed in *rrm4Δ* strains, loss of Grp1 did not cause an increased amount of bipolar cells as it is characteristic for defects in microtubule-dependent transport (see *rrm4Δ* hyphae for comparison; Fig. 1B-C; Haag et al., 2017). On the contrary, under optimal growth conditions hyphae were significantly longer (Fig. 1B-C), and the length of empty sections at the basal pole was increased (Fig. 1D; Fig. S1H). Hence, the coordination of hyphal growth may be disturbed in the absence of Grp1. In order to further

bioRxiv preprint doi: https://doi.org/10.1101/418079; this version posted September 14, 2018. The copyright holder for this preprint (which was not certified by peer review) is the author/funder, who has granted bioRxiv a license to display the preprint in perpetuity. It is made available under aCC-BY-NC-ND 4.0 International license.

support this, we stressed hyphae three hours post induction (h.p.i.) of hyphal growth with the cell wall inhibitor CFW. In comparison to wild type hyphae, we observed a strongly increased number of *grp1Δ* hyphae with abnormal shapes (86%), indicating that cell wall integrity might be affected (Fig. 1E-F).

In summary, loss of Grp1 affects both yeast-like and hyphal growth. During the latter, Grp1 seems to be crucial for the correct coordination of cell wall expansion, which becomes particularly apparent during stress conditions.

Grp1 is a novel component of endosomal mRNA transport

To analyse the subcellular localisation of Grp1, we generated AB33 strains expressing Grp1 fused at its C-terminus to Gfp by homologous recombination. The functional Grp1-Gfp version accumulated in the cytoplasm as well as in the nucleus of hyphae. In comparison, the poly(A)-binding protein Pab1-Gfp was absent from the nucleus, suggesting that this localisation pattern is specific for Grp1 (Fig. 2A). Importantly, a subpopulation of Grp1-Gfp moved bi-directionally in the cytoplasm with a velocity comparable to Rrm4-Gfp and Pab1-Gfp, which are known to shuttle on early endosomes (Fig. 2A-B; Supplemental Video 1).

To verify that Grp1 shuttles on Rrm4-positive endosomes, we performed dynamic co-localisation studies using dual-view technology (Baumann, Takeshita et al., 2015). We generated AB33 strains co-expressing Grp1-Gfp and Rrm4 fused C-terminally to the red fluorescent protein Tag-Rfp (tRfp; Merzlyak, Goedhart et al., 2007). For comparison, we used a strain expressing Pab1 fused to the red fluorescent protein mCherry (Campbell, Tour et al., 2002, König et al., 2009). Analysing hyphae 6 h.p.i. 99% of processive Grp1-Gfp signals co-migrated with Rrm4-tRfp, revealing extensive co-localisation of both proteins in shuttling units (Fig. 2C-D; Supplemental Video 2). Consistently, 97% of processive Grp1-Gfp signals co-migrated with Pab1-mCherry, indicating that Grp1, like Pab1, was present on almost all Rrm4-positive endosomes (Fig. 2C-D; Supplemental Videos 3-4). Thus, Grp1 appears to be a

bioRxiv preprint doi: https://doi.org/10.1101/418079; this version posted September 14, 2018. The copyright holder for this preprint (which was not certified by peer review) is the author/funder, who has granted bioRxiv a license to display the preprint in perpetuity. It is made available under aCC-BY-NC-ND 4.0 International license.

novel component of endosomal mRNPs that might already be recruited to transport mRNPs in the nucleus.

The endosomal localisation of Grp1 depends on Rrm4

To investigate whether Grp1 has an influence on the shuttling of Rrm4-positive endosomes, we studied Rrm4 movement in *grp1Δ* strains. Loss of Grp1 altered neither processive Rrm4-Gfp movement nor the velocity of the respective endosomes (Fig. 2E-F; Supplemental Video 5). Vice versa, studying Grp1-Gfp movement in the absence of Rrm4 revealed that its endosomal localisation depended on Rrm4 (Fig. 2G). Importantly, similar to Pab1-Gfp, a gradient of Grp1-Gfp was formed in *rrm4Δ* hyphae, with a decreasing signal intensity towards the growing apex (Fig. 2H-I; König et al., 2009). Similar to Pab1, which is expected to associate with almost all poly(A) tails of mRNAs (Hogan, Riordan et al., 2008), Grp1 might therefore be distributed in association with many mRNAs (see below).

To test whether Grp1-Gfp binds to endosomes in an mRNA-dependent manner, we generated AB33 strains expressing Rrm4^{mR123}-tRfp. This Rrm4 variant carried point mutations in the RNP1 regions of RRM domains 1-3 causing a reduced RNA binding activity and loss of function of Rrm4 (Becht et al., 2006). In dual-view experiments we observed that Grp1-Gfp like Pab1-Gfp no longer shuttled in the presence of Rrm4^{mR123}-tRfp (Fig. 2J). Thus, the localisation of Grp1 depends on the presence of functional Rrm4, more precisely on its capability to bind RNA. In summary, we identified Grp1 as a novel component of endosomal mRNPs whose shuttling on Rrm4-positive endosomes depended on Rrm4 and mRNA.

Rrm4 and Grp1 share thousands of target transcripts

In order to learn more about the function of the two endosomal mRNP components Rrm4 and Grp1 during hyphal growth, we performed a comparative transcriptome-wide analysis of their RNA binding behaviour using individual-nucleotide resolution UV crosslinking and

bioRxiv preprint doi: https://doi.org/10.1101/418079; this version posted September 14, 2018. The copyright holder for this preprint (which was not certified by peer review) is the author/funder, who has granted bioRxiv a license to display the preprint in perpetuity. It is made available under aCC-BY-NC-ND 4.0 International license.

immunoprecipitation (iCLIP; König, Zarnack et al., 2010). For application with fungal RBPs, we had to modify a number of steps in the iCLIP protocol (Huppertz, Attig et al., 2014; Fig. S2; see Materials and methods). One major challenge was the high RNase and protease activity in fungal cell extracts that resulted in a low yield of crosslinked protein-RNA complexes and short mRNA fragments. The most critical changes to the protocol came with the fast processing of crosslinked material and the identification of the optimal UV-C irradiation dose (Fig. S2).

Using the improved protocol, we found that Rrm4-Gfp and Grp1-Gfp displayed substantial crosslinking to RNA *in vivo* (compared to Gfp control; Fig. 3A). As expected, the RNA signal was dependent on UV-C irradiation and sensitive to RNase I digestion. Upon iCLIP library preparation, we obtained more than 100 million sequencing reads, corresponding to 4.7 x 10^6 and 14.8 x 10^6 crosslink events for Rrm4 and Grp1, respectively (Fig. S3A-B). Reproducibility between two replicate experiments was high for both proteins, demonstrating the quality of the obtained data set (Pearson correlation coefficient > 0.96, p value < 2.22e-16; Fig. S3C).

Consistent with the abundance of both proteins, the crosslink events accumulated into thousands of clusters that spread across major parts of the transcriptome (Fig. S3A). In order to focus on the most prominent sites, we used the crosslink frequency within each cluster relative to the background signal within the same transcript to determine the 25% most prominent binding sites for Rrm4 and Grp1 ('signal-over-background'; see Materials and methods). This procedure identified a total of 6,412 binding sites for Rrm4 and 6,478 binding sites for Grp1, residing in 3,262 and 3,165 target transcripts, respectively (Fig. 3B). This represented a substantial fraction of the about 6,700 protein-encoding genes in the *U. maydis* genome (Kämper, Kahmann et al., 2006). Extensive endosomal transport of mRNA is consistent with a role in evenly distributing mRNAs throughout hyphae (see Discussion).

bioRxiv preprint doi: https://doi.org/10.1101/418079; this version posted September 14, 2018. The copyright holder for this preprint (which was not certified by peer review) is the author/funder, who has granted bioRxiv a license to display the preprint in perpetuity. It is made available under aCC-BY-NC-ND 4.0 International license.

Comparing Rrm4 and Grp1 revealed a large overlap of 2,114 target transcripts that were conjointly bound by both proteins (Fig. 3B-C, Supplemental Table S1; see below). In this shared target set, we observed an enrichment for functional categories like mitochondrion, vesicle transport and cytoskeleton (Fig. 3D). Moreover, we found several known Rrm4 target transcripts, including for instance all four *septin* mRNAs (Fig. 3C, 3E). Binding sites of Rrm4 and Grp1 in the *septin* mRNAs were almost exclusively located in the 3´ untranslated region (UTR), consistent with the hypothesis that these mRNAs are transported in a translationally active state (Zander et al., 2016; see Discussion). *cts1* mRNA, another known target of the Rrm4 transport machinery (Koepke et al., 2011), also carried binding sites of both RBPs in the 3´ UTR (Fig. S3D).

To assess the function of target mRNAs that are specifically recognised by only one of the two RBPs, we applied more stringent criteria to define 280 and 520 transcripts that were uniquely bound by Rrm4 and Grp1, respectively (Fig. S3E, Supplemental Tables S2-S3). While the Rrm4-unique set displayed no clear trend, the Gpr1-unique set showed an enrichment for mRNAs encoding nuclear proteins that were involved in transcriptional regulation and chromatin remodelling (Fig. 3D). Although these mRNAs were expressed and bound by Grp1, they were most likely not transported by the Rrm4 machinery and would hence remain around the nucleus. This could facilitate their perinuclear translation and an efficient nuclear import of the translation products, as being described in mammalian cells for transcription factors like c-Myc or for metallothionin (Chabanon, Mickleburgh et al., 2005, Levadoux, Mahon et al., 1999).

In summary, the comparative iCLIP approach revealed that Grp1 and Rrm4 conjointly bind thousands of shared target mRNAs. These offer a comprehensive view on the full spectrum of cargo mRNAs transported by the endosomal mRNP transport machinery in *U. maydis*.

bioRxiv preprint doi: https://doi.org/10.1101/418079; this version posted September 14, 2018. The copyright holder for this preprint (which was not certified by peer review) is the author/funder, who has granted bioRxiv a license to display the preprint in perpetuity. It is made available under aCC-BY-NC-ND 4.0 International license.

Rrm4 binds to functionally important sites of target transcripts

Studying the distribution of binding sites in different transcript regions revealed that Rrm4 and Grp1 preferentially bound in the 3´ UTR (Fig. 4A). Within this region, both proteins frequently bound in close proximity, with 51% of Rrm4 binding sites directly overlapping with a Grp1 binding site (compared to only 5% in the open reading frame, ORF; Fig. 4B-C). Thus, the cargo mRNAs of the transport mRNPs are often conjointly recognised by both RBPs in the 3´ UTR.

In contrast to Grp1 that was almost exclusively attached to the 3´ UTR, Rrm4 bound a substantial fraction of target mRNAs within the ORF (1,315 cases; Fig. 4A, 4C). Taking a closer look at the binding pattern of Rrm4 along ORFs, we observed an increased binding at the start and stop codons of selected target mRNAs (Fig. 4D). Whereas only two transcripts harboured a Grp1 binding site at the start codon, Rrm4 binding sites overlapped the start codon in 47 cases, like in the transcript encoding the translation initiation factor Sui1 (UMAG _02665; Fig. 4E; Supplemental Table S4). Binding of Rrm4 at the start codon of these mRNAs might interfere with translation initiation, suggesting that these mRNAs may be transported in a translationally silent state. Of note, the *rrm4* mRNA itself exhibited Rrm4 binding sites around the start codon, hinting at a potential autoregulation (Fig. S3D).

Even more prominently than at start codons, we observed a strong accumulation of Rrm4 binding sites at the stop codons of multiple target transcripts (291 cases; Fig. 4D-E; Supplemental Table S5). These included, for example, both subunits of cytoplasmic dynein (Dyn1 and Dyn2; Straube, Enard et al., 2001). Furthermore, the stop codon-bound targets were significantly enriched for mRNAs encoding mitochondrial proteins, including for instance the majority of nucleus-encoded subunits and accessory components of the F_OF_1-ATPase (Fig. S4). Through binding at the stop codon, Rrm4 might influence translation termination for distinct targets.

bioRxiv preprint doi: https://doi.org/10.1101/418079; this version posted September 14, 2018. The copyright holder for this preprint (which was not certified by peer review) is the author/funder, who has granted bioRxiv a license to display the preprint in perpetuity. It is made available under aCC-BY-NC-ND 4.0 International license.

In essence, the high-resolution mapping of binding sites for the two endosomal RBPs Rrm4 and Grp1 revealed (i) that both proteins conjointly bind in the 3´ UTR, and (ii) that Rrm4 additionally recognises binding sites in the ORF and at translational landmarks like start and stop codons.

Rrm4 specifically recognises the motif UAUG via its third RRM

In order to address the RNA sequence specificity of both RBPs, we used the motif analysis algorithm DREME (Bailey, 2011) to search for sequence motifs in a 30-nt window around the RBP binding sites. This analysis retrieved UAUG as the most significantly enriched sequence motif at Rrm4 binding sites (Fig. 5A). Analysing the relative positioning of the motif showed that more than one third of all Rrm4 binding sites harboured a UAUG motif precisely at the centre of the binding site (2,201 out of 6,412; Fig. 5B). The motif did not accumulate at Grp1 binding sites, supporting the notion that the motif was specifically recognised by Rrm4. Notably, the Rrm4 binding sites with UAUG showed stronger relative binding than those lacking the motif (Fig. 5C), suggesting a tight interaction of Rrm4 with the UAUG-associated binding sites.

A similar sequence analysis of the Grp1 binding sites initially suggested the sequence UGUA as a potential recognition motif (Fig. S5A). However, the same motif also frequently occurred at Rrm4 binding sites and showed no clear positioning relative to the Grp1 binding sites (Fig. S5B), making it questionable whether it was directly involved in the RNA recognition of Grp1. We therefore did not pursue this motif further.

In order to independently verify that Rrm4 specifically recognises the sequence motif UAUG, we applied the yeast three-hybrid assay (Fig. 5D). We previously used this approach to successfully identify SELEX-derived RNA aptamers that were recognised by the third RRM domain of Rrm4 *in vivo* (RRM3; König, Julius et al., 2007). Intriguingly, two RNA aptamers, SELEX-A1 and SELEX-B1, contained the UAUG motif. We chose SELEX-A1

bioRxiv preprint doi: https://doi.org/10.1101/418079; this version posted September 14, 2018. The copyright holder for this preprint (which was not certified by peer review) is the author/funder, who has granted bioRxiv a license to display the preprint in perpetuity. It is made available under aCC-BY-NC-ND 4.0 International license.

(Fig. 5E; König et al., 2007) to mutate the UAUG motif and tested RNA binding using the yeast three-hybrid assay. In contrast to the initial SELEX-A1 aptamer, the mutant version was no longer recognised by Rrm4 (Fig. 5F; Fig. S5C). Consistent with earlier results, mutating the third RRM domain of Rrm4 gave similar results in the context of the initial SELEX-A1 aptamer (König et al., 2007). Thus, our computational and experimental analyses indicate that Rrm4 specifically recognises the sequence motif UAUG via its third RRM domain.

Interestingly, Rrm4 binding sites in the whole ORF region showed a strong enrichment for the Rrm4 motif UAUG (Fig. 5H), such that 61% of all ORF binding sites harboured UAUG. In line with this, the vast majority of start codon-associated binding sites had the start codon AUG into an UAUG motif (88%, Fig. 5H), whereas stop codons seem to be recognised differently (UGA overlaps with UAUG i.e. UA<u>UGA</u>; but UAA was the most common stop codon, 55%, Fig. 5I). Since UAUG-containing binding sites showed particularly strong Rrm4 binding (Fig. 3C; as examples, see *cdc3* and *cdc12* in Fig. 3C, 3E), Rrm4 appears to exhibit a tight association with the ORF via its third RRM domain. Uniting these observations, we hypothesised that Rrm4 simultaneously recognised multiple regions of the same cargo mRNAs. In line with this notion, we found that transcripts with a Rrm4 binding site in the 3′ UTR were significantly enriched for a second Rrm4 binding site in the ORF (663 out of 1,703 transcripts with at least two Rrm4 binding sites; p value < 2.22e-16, Fisher's exact test). In 69% of these cases, the ORF binding site harboured UAUG, and in 56%, the 3′ UTR binding site of Rrm4 overlapped with a Grp1 binding site. Taken together, these observations would be consistent with a model that Rrm4 binds with its RRM domains RRM1 and/or RRM2 close to Grp1 in the 3′ UTR and via its third RRM domain to a UAUG-containing binding site in the ORF (Fig. 6).

bioRxiv preprint doi: https://doi.org/10.1101/418079; this version posted September 14, 2018. The copyright holder for this preprint (which was not certified by peer review) is the author/funder, who has granted bioRxiv a license to display the preprint in perpetuity. It is made available under aCC-BY-NC-ND 4.0 International license.

Discussion

At present, a small number of high-throughput studies provided a global view on transported and localised mRNAs. In oocytes and embryos from fruit fly, transcriptome-wide RNA *in situ* hybridisation approaches revealed that the majority of transcripts exhibit a defined localisation pattern (Jambor, Surendranath et al., 2015, Lécuyer, Yoshida et al., 2007). In neuronal cells, the localised transcriptome and proteome have also been compiled (Cajigas, Tushev et al., 2012, Rangaraju, Tom Dieck et al., 2017). However, it is still unclear (i) how these cargo mRNAs reach their destination, (ii) which RBPs mediate their transport, and (iii) what are the precise interaction sites within the target mRNAs. Here, we applied iCLIP to study the newly identified endosomal RBP Grp1 and the key transport RBP Rrm4 during endosomal mRNP transport in *U. maydis*. According to the best of our knowledge, this is the first detailed iCLIP analysis of mRNA transport.

The GQ-rich RNA-binding protein Grp1 is a novel component of endosomal mRNPs

The small GQ-rich protein Grp1 shares similarity with other glycine-rich RBPs from humans and plants. A characteristic feature of this conserved class of RBPs is an N-terminal RRM domain followed by a glycine-rich low-complexity sequence that is typical for intrinsically disordered regions (IDRs). In RBPs, IDRs mediate the assembly of membrane-less organelles through phase transitions (Calabretta & Richard, 2015), and this assembly is important, for example, during splicing (Ying, Wang et al., 2017). Interestingly, IDRs have also been implicated in the formation of RNA granules for neuronal RNA transport (Jung, Yoon et al., 2012, Kato, Han et al., 2012).

Small glycine-rich RBPs function in a wide variety of biological processes. The plant protein *At*GRP7, for example, is involved in cold stress adaption, osmotic stress response, circadian rhythm and plant immunity (Ciuzan, Hancock et al., 2015, Kang et al., 2013, Meyer, Koster et al., 2017). Human CIRBP regulates telomerase activity, and the human cold shock

bioRxiv preprint doi: https://doi.org/10.1101/418079; this version posted September 14, 2018. The copyright holder for this preprint (which was not certified by peer review) is the author/funder, who has granted bioRxiv a license to display the preprint in perpetuity. It is made available under aCC-BY-NC-ND 4.0 International license.

protein RBM3 is involved in translational reprogramming during the cooling response of neuronal cells (Bastide, Peretti et al., 2017, Peretti, Bastide et al., 2015, Zhu et al., 2016). Globally, these proteins might function as RNA chaperones that prevent the formation of aberrant RNA secondary structures under stress conditions (Ciuzan et al., 2015, Kim, Park et al., 2007).

In this study, we observe that loss of the fungal orthologue Grp1 causes aberrant alterations of the hyphal growth programme. Under optimal conditions *grp1Δ* hyphae grow significantly longer, suggesting an unusual acceleration of cell wall formation. Moreover, cell wall stress revealed clear abnormal morphologies in comparison to wild type. Consistent with a role in hyphal growth, Grp1 shuttles on Rrm4-positive endosomes that are the main transport units for long-distance transport of mRNAs in hyphae. Moreover, Grp1 and Rrm4 conjointly bind in the 3´ UTRs of thousands of target mRNAs (Fig. 6A, see below). We therefore conclude that the potential RNA chaperone Grp1 is involved in efficient transport of mRNPs, in particular under suboptimal conditions.

It is of note that the RRM protein Hrb27C (Hrp48) from fruit fly with a related domain architecture containing two N-terminal RRMs followed by a C-terminal GQ-rich region was found as an mRNP component during transport of *oskar* and *gurken* mRNAs (Goodrich, Clouse et al., 2004, Huynh, Munro et al., 2004, Yano, Lopez de Quinto et al., 2004). Hence, the presence of small glycine-rich RBPs in transport mRNPs might be preserved across organisms.

Endosomal RBPs recognise a broad spectrum of cargo mRNAs

In order to obtain a comprehensive view on the *in vivo* mRNA targets of an RBP, UV crosslinking techniques are currently the method of choice (König, Zarnack et al., 2012, Van Nostrand, Pratt et al., 2016, Zarnegar, Flynn et al., 2016). Here, we applied iCLIP to study fungal mRNA transport. A strength of our approach was the use of strains expressing

bioRxiv preprint doi: https://doi.org/10.1101/418079; this version posted September 14, 2018. The copyright holder for this preprint (which was not certified by peer review) is the author/funder, who has granted bioRxiv a license to display the preprint in perpetuity. It is made available under aCC-BY-NC-ND 4.0 International license.

functional Gfp-tagged versions of Grp1 and Rrm4 using homologous recombination to avoid overexpression artefacts. For application in fungi, we had to improve several steps (Huppertz et al., 2014), of which optimising the dose and duration of UV-C irradiation was most critical. Thereby, we were able to obtain a transcriptome-wide view of the cargo mRNAs, including their interaction sites with cognate RBPs at single nucleotide resolution.

Comparing two distinct RBPs present in endosomal mRNPs enabled us to disentangle the precise binding behaviour of the two co-localising RBPs. We identified more than 2,000 shared target transcripts, covering a substantial amount of the approximately 6,700 annotated protein-coding genes (Kämper et al., 2006; http://pedant.helmholtz-muenchen.de/index.jsp; ORF update 2016.11.08). The broad target spectrum of endosomal mRNA transport fits with earlier observations that Rrm4 transported all mRNAs under investigation, albeit with different processivity of transport (König et al., 2009). Moreover, loss of Rrm4 impairs the global mRNA distribution in hyphae, indicated by a disturbed subcellular distribution of the poly(A)-binding protein Pab1 (König et al., 2009). Thus, one function of the endosomal mRNA transport machinery might be the equal distribution of mRNPs to supply all parts of the hyphae with mRNAs. This might be particularly important for those parts that are distant from the mRNA-synthesising nucleus. Such a universal mRNA transport mode resembles the "sushi belt model" in neuronal cells, in which the shuttling of mRNPs by active transport along microtubules is thought to distribute mRNAs throughout the dendrite to serve synapses that are in demand of mRNAs (Doyle & Kiebler, 2011). Furthermore, since many mRNAs in *U. maydis* appear to be transported in a translationally active state (see below), this mRNA distributer function would also disclose the mechanism of how ribosomes are transported by endosomes, as observed previously (Higuchi, Ashwin et al., 2014).

Notably, we found that most nuclear-encoded subunits and accessory components of mitochondrial F_OF_1 ATPase are targets of endosomal mRNP transport in *U. maydis*. Consistent with the idea that a precise spatiotemporal regulation of translation might be

bioRxiv preprint doi: https://doi.org/10.1101/418079; this version posted September 14, 2018. The copyright holder for this preprint (which was not certified by peer review) is the author/funder, who has granted bioRxiv a license to display the preprint in perpetuity. It is made available under aCC-BY-NC-ND 4.0 International license.

important for efficient mitochondrial protein import, we observed that the abundance of Atp4 is reduced in *rrm4Δ* hyphae (Koepke et al., 2011). These results agree with previous findings that the 3´ UTR of *ATP2* mRNA from *S. cerevisiae* is important for efficient mitochondrial uptake of mature Atp2p (Margeot, Blugeon et al., 2002). A close link between RNA biology and mitochondrial protein import is thus an emerging theme in mitochondrial biology (Gehrke, Wu et al., 2015, Gold, Chroscicki et al., 2017, Lesnik, Golani-Armon et al., 2015, Sen & Cox, 2016, Zhang, Chen et al., 2016).

Distinct binding patterns of Rrm4 may allow orchestration of mRNA transport and translation

The positional information obtained by single nucleotide resolution was essential to uncover the precise binding behaviour of the involved RBPs. In the majority of cases, Rrm4 binds together with Grp1 in the 3´ UTR (1,700 transcripts; Fig. 6A). The vicinity of these binding sites to the poly(A) tail fits the previous observation that the endosomal adaptor protein Upa1 interacts with both Rrm4 and Pab1 (Pohlmann, Baumann et al., 2015). While translating ribosomes would potentially remove RBPs from the ORF (Halstead, Lionnet et al., 2015), such binding in the 3´ UTR, as seen e.g. on all four *septin* mRNAs, would allow simultaneous translation and transport of mRNAs. Consistently, we have recently provided evidence that endosome-coupled translation of *septin* mRNAs mediates endosomal assembly and transport of heteromeric septin complexes (Baumann et al., 2014, Zander et al., 2016). Since transport of translationally active mRNAs has recently been observed in neurons (Wu, Eliscovich et al., 2016), this mode of transport might be more widespread than currently anticipated.

Our transcriptome-wide RNA binding maps illustrate an intriguing binding pattern of Rrm4 at translational landmark sites, indicating an intimate connection of endosomal mRNP transport and translation in *U. maydis* (Fig. 6A): First, in over 1,000 target transcripts Rrm4 binds within the ORF, indicating that it may be involved in stalling translational elongation.

bioRxiv preprint doi: https://doi.org/10.1101/418079; this version posted September 14, 2018. The copyright holder for this preprint (which was not certified by peer review) is the author/funder, who has granted bioRxiv a license to display the preprint in perpetuity. It is made available under aCC-BY-NC-ND 4.0 International license.

Notably, a similar mechanism was suggested in neurons, in which a subset of mRNAs are translationally stalled during transport (Graber, Hebert-Seropian et al., 2013). Similar to Rrm4, the neuronal RBP FMR1 binds its translationally stalled target mRNAs preferably in the coding sequence (Darnell, Van Driesche et al., 2011). Second, in about 50 and 300 cases, respectively, Rrm4 precisely binds at the start and stop codons of the target transcripts, suggesting modulation of translation initiation and termination. At start codons and within the ORF, the Rrm4 binding sites frequently harboured UAUG. This motif is recognised by the third RRM domain of Rrm4, mutations of which previously led to strongly reduced overall RNA binding of Rrm4 (Becht et al., 2006). In accordance with its ELAV-type domain organisation, we therefore propose that Rrm4 binds UAUG-containing binding sites via its third RRM to influence translation (Fig. 6B), while the two tandem RRMs (RRM1/2) bind the target mRNAs in the 3´ UTR, possibly together with Grp1 (Fig. 6B). Since Rrm4 variants with mutations in RRM3 did not show a phenotype with respect to hyphal growth (Becht et al., 2006), the translational regulation during endosomal mRNP transport may be an additive and used for fine tuning, but not essential. In contrast, RRM1 was crucial for hyphal growth, and mutations in this domain resulted in reduced endosomal shuttling of Pab1 as well as *cdc3* mRNA (Baumann et al., 2014). These observations are in line with the notion that the tandem RRMs of Rrm4 might mediate the recognition of target mRNAs for transport, possibly via binding in the 3´ UTR.

In essence, our comprehensive transcriptome-wide view on endosomal mRNA transport revealed the precise positional deposition of co-localising RBPs during transport. The key RBP Rrm4 exhibits a particular binding behaviour by recognising distinct landmarks of translation in target mRNAs. Thereby, translation and transport might be intimately coupled and precisely synchronised for the specific expression needs of each target transcript.

bioRxiv preprint doi: https://doi.org/10.1101/418079; this version posted September 14, 2018. The copyright holder for this preprint (which was not certified by peer review) is the author/funder, who has granted bioRxiv a license to display the preprint in perpetuity. It is made available under aCC-BY-NC-ND 4.0 International license.

Materials and methods

Plasmids, strains and growth conditions

Cloning was done using *E. coli* K-12 derivate Top10 (Life Technologies, Carlsbad, CA, USA). All strains were constructed by the transformation of cells with linearised plasmids, and homologous integration events were verified by Southern blot analysis (Brachmann, König et al., 2004). Genomic DNA of wild type strain UM521 (*a1b1*) served as template for PCR amplifications unless noted otherwise. Proteins were tagged with eGfp (enhanced green fluorescent protein; Clontech, Mountain View, CA, USA), Tag-Rfp or mCherry (Merzlyak et al., 2007, Shaner, Campbell et al., 2004). Plasmid sequences are available upon request. The accession numbers of *U. maydis* genes used in this study are: *rrm4* (UMAG_10836), *grp1* (UMAG_02412), *pab1* (UMAG_03494). Detailed information is supplied in Supplemental Tables S8-S9. The conditions used for cultivation of *U. maydis* are described elsewhere (Brachmann et al., 2004). For the induction of filamentous growth of lab strain AB33 and derivates, cultures were grown to an OD_{600} of 0.5 in complete medium supplemented with 1% glucose (CM-glc) and shifted to nitrate minimal medium supplemented with 1% glc (NM-glc). The growth curves of *U. maydis* strains were recorded by cultivating strains in CM-glc at 28°C and measuring the OD_{600} every 2 h.

Multiple sequence alignments

Orthologous proteins were identified using BLAST P (https://blast.ncbi.nlm.nih.gov/blast/). Clustal W and GeneDoc 2.6 were used for multiple amino acid sequence alignment and graphical representation, respectively (Larkin, Blackshields et al., 2007).

Colony morphology, temperature stress and cell wall stress

For growth on solid media, cell suspensions (OD_{600} of 0.5) were inoculated onto respective plates at 28°C. Colony morphology was tested on CM (1% glc) medium. Temperature stress

bioRxiv preprint doi: https://doi.org/10.1101/418079; this version posted September 14, 2018. The copyright holder for this preprint (which was not certified by peer review) is the author/funder, who has granted bioRxiv a license to display the preprint in perpetuity. It is made available under aCC-BY-NC-ND 4.0 International license.

was analysed on CM (1% glc) medium, incubated at 28°C, 20°C or 16°C. Cell-wall stress was analysed by supplementing CM (1% glc) medium with 50 µM Calcofluor White (Sigma-Aldrich, Taufkirchen, Germany) or 40 µg/ml Congo Red (Sigma-Aldrich). All plates were kept for at least 48 h at the required temperature. The set-up used to acquire images was described before (Pohlmann et al., 2015). To analyse cell wall stress in hyphae, 2.5 µM Calcofluor White was added to cultures 3 hours post induction (h.p.i) and incubated for an additional 2 h.

Microscopy and image processing

The microscope set-ups and dual-colour imaging were used as described before (Baumann et al., 2012, Baumann et al., 2015, Baumann, Zander et al., 2016). Gfp and tagRfp or mCherry fluorescence was simultaneously detected using a two-channel imager (DV2, Photometrics, Tucson, AZ, USA). All images and videos were acquired and analysed using Metamorph (Versions 7.7.0.0 and 7.7.4.0; Molecular Devices, Sunnyvale, CA, USA).

Cell length was assessed by measuring the length of single cells from pole-to-pole. For hyphae, empty sections were not included in the measurements. The length of empty sections was assessed by measuring the distance from septum to septum of the first empty section at the distal pole of hyphae. Cell wall defects induced by Calcoflour White were quantified by manually scoring for the presence of abnormal cell wall shapes.

For the analysis of co-localisation and velocity of moving signals the acquired videos were converted to kymographs using Metamorph. Co-localisation was assessed by quantifying kymographs acquired by dual-colour imaging. Changes in direction were counted as individual signals. Processive signals (distance travelled > 5 µm) were counted manually. Velocity was only measured for processive signals (movement > 5 µm). For all quantifications, at least three independent experiments were analysed. Statistical analysis was performed using Prism5 (Graphpad, La Jolla, CA, USA).

bioRxiv preprint doi: https://doi.org/10.1101/418079; this version posted September 14, 2018. The copyright holder for this preprint (which was not certified by peer review) is the author/funder, who has granted bioRxiv a license to display the preprint in perpetuity. It is made available under aCC-BY-NC-ND 4.0 International license.

The gradient of Grp1-Gfp, Pab1-Gfp and Gfp in the presence and absence of Rrm4 was quantified by measuring the fluorescence intensity in a previously specified region of interest (ROI; ROI1 in vicinity to the nucleus and ROI2 at the hyphal tip). The fluorescence close to the nucleus was then set in relation to the signal intensity at the tip. For all quantifications, at least three independent experiments were analysed. Statistical analysis was performed using Prism5 (Graphpad, La Jolla, CA, USA).

iCLIP experiments

The iCLIP protocol was modified from the one described in Huppertz et al., 2014. (i) The initial two-step Tap tag purification (König et al., 2009) was switched to single-step purification using Rrm4-Gfp-expressing strains and Gfp-trap immunoprecipitation (Rothbauer, Zolghadr et al., 2008; ChromoTek, Martinsried, Germany). (ii) For UV-C crosslinking, cells were irradiated continuously in a single session. (iii) RNase I (1/10 dilution, 16 minutes, 37°C) was used for the controls (Fig. 3A). The addition of DNase and RNase I was omitted from the samples used for iCLIP library preparation. The addition of external RNases was unnecessary due to the high fungal RNase activity. The experiments were performed with 150 ml cultures grown to an $OD_{600} = 0.5$ in CM (1% glc) and then shifted to NM-glc. After 6 h hyphae were harvested by centrifugation at 7,500 rpm for 10 min at 4°C and the pellet resuspended in 15 ml ice-cold PBS. For UV-C crosslinking, the cell suspension was split into 3x 5 ml and kept on ice. Cells were irradiated with 200 mJ/cm^2 at 254 nm (Biolink UV-Crosslinker, Vilber-Lourmat, Eberhardzell, Germany), pooled in a 50 ml tube, and hyphae were harvested by centrifugation at 7,500 rpm for 10 min at 4°C. Hyphae were resuspended in 6 ml lysis buffer (50 mM Tris-HCl, pH 7.4, 100 mM NaCl, 1% Nonidet P-40, 0.1% SDS, 0.5% sodium deoxycholate) supplemented with proteinase inhibitors per 10 ml lysis buffer: 2× Complete protease inhibitor EDTA-free (Roche Diagnostics, Mannheim, Germany), 1 mM reduced DTT (GERBU, Heidelberg, Germany), 1 mM PMSF (Sigma), 0.75

bioRxiv preprint doi: https://doi.org/10.1101/418079; this version posted September 14, 2018. The copyright holder for this preprint (which was not certified by peer review) is the author/funder, who has granted bioRxiv a license to display the preprint in perpetuity. It is made available under aCC-BY-NC-ND 4.0 International license.

µg/µl heparin (Sigma), 5.25 ng/µl pepstatin A (Sigma) and 15 µl SUPERase-In (20 U/µL; Thermo Fisher Scientific, Darmstadt, Germany). Cell lysis was performed in a Retsch ball mill (d=12 mm; MM400; Retsch, Haan, Germany) 3 times for 10 min at 30 Hz while keeping samples frozen using liquid nitrogen. All following steps were performed at 4°C. The cell lysate was harvested by centrifugation at 7,500 rpm for 10 min at 4°C, pooled, and the protein-RNA complexes purified by using 60 µl GFP-Trap_MA beads (Chromotek; Rothbauer et al., 2008). The beads were pre-washed 3 times with 500 µl ice-cold lysis buffer (without inhibitors), the cell lysate added and incubated for 1 h at 4°C. All following washing steps of the beads were performed with 900 µl of the respective buffer. The beads were washed 3 times with high-salt wash buffer and 4 times with PNK buffer. 3' end RNA dephosphorylation, L3 adapter ligation, 5' end phosphorylation, SDS-PAGE and nitrocellulose transfer were performed as described (Huppertz et al., 2014) with minor changes implemented. 50% instead of 20% of the sample were radioactively labelled for 10 min at 37°C and the labelled beads were washed once with PNK buffer before they were combined with the unlabelled beads. The beads were diluted in 80 µl 1× NuPAGE LDS loading buffer (NP0007, Invitrogen, Darmstadt, Germany) with 0.1 M DTT. The protein-RNA complexes were separated at 180 V for 70 min on a 4-12% NuPAGE Bis-Tris gel (1x MOPS running buffer, NP0001, Invitrogen) and transferred onto a nitrocellulose membrane. Gfp was detected using monoclonal α-GFP antibodies (clones 7.1 and 13.1; Sigma) and a mouse IgG HRP conjugate (H+L; Promega, Madison, WI, USA) as first and secondary antibody, respectively. Peroxidase activity was determined using the AceGlow blotting detection system (Peqlab, Erlangen, Germany).

Labelled RNA was detected by overnight exposure of X-ray films at -80°C. All following steps were performed as described before (Huppertz et al., 2014). To avoid over-amplification of the cDNA library, the optimal PCR cycle number was tested for each individual protein in every experiment (PCR cycler, PTC-200, MJ Research, St. Bruno,

bioRxiv preprint doi: https://doi.org/10.1101/418079; this version posted September 14, 2018. The copyright holder for this preprint (which was not certified by peer review) is the author/funder, who has granted bioRxiv a license to display the preprint in perpetuity. It is made available under aCC-BY-NC-ND 4.0 International license.

Quebec, Canada). For all Grp1 and Gfp replicates, 18 PCR cycles were determined, and for the Rrm4 sample, 18 and 22 PCR cycles were determined for the two replicates, producing PCR products of around 150 nt (cDNA insert = 20-30 nt; L3 adapter, RT-primer and P3/P5 Solexa primers = 128 nt).

The iCLIP libraries were multiplexed and sequenced on an Illumina HiSeq 2500 (San Diego, CA, USA; 51-nt reads, single-end), yielding a total of 118 million reads.

iCLIP data processing

All bioinformatics analyses are based on the *U. maydis* 521 genome sequence (original PEDANT database name p3_t237631_Ust_maydi_v2GB) and the associated gene annotation (version p3_t237631_Ust_maydi_v2GB.gff3; both downloaded from ftp://ftpmips.gsf.de/fungi/Ustilaginaceae/Ustilago_maydis_521/). We extended all genes by 300 nt on either side to include potential 5´ and 3´ UTR regions which are currently not annotated in the *U. maydis* genome. For manual annotation of transcript ends, RNASeq data (AB33 hyphae, 6 h.p.i.) were used, and transcript ends were defined at the position where read coverage dropped below 10.

Basic quality checks were applied to all sequenced reads using FastQC (https://www.bioinformatics.babraham.ac.uk/projects/fastqc/). Afterwards, iCLIP reads were filtered based on sequencing quality (Phred score) in the barcode region, keeping only reads with at most one position with a Phred score < 20 in the experimental barcode (positions 4 to 7) and without any position with a Phred score < 17 in the random barcode (positions 1 to 3 and 8 to 9). The reads were then de-multiplexed based on the experimental barcode at positions 4 to 7 using Flexbar (version 2.4, GitHub, San Francisco, CA, USA) without allowing mismatches (Dodt, Roehr et al., 2012). The following analysis steps were applied to all individual samples: remaining adapter sequences were trimmed from the 3´ end of the reads using Flexbar (version 2.4) allowing one mismatch in 10 nt, requiring a minimal overlap

bioRxiv preprint doi: https://doi.org/10.1101/418079; this version posted September 14, 2018. The copyright holder for this preprint (which was not certified by peer review) is the author/funder, who has granted bioRxiv a license to display the preprint in perpetuity. It is made available under aCC-BY-NC-ND 4.0 International license.

514 of 1 nt between read and adapter as well as removing all reads with a remaining length of less
515 than 24 nt (including the 9-nt barcode). The first 9-nt of each read containing the barcode
516 were trimmed off and added to the read name in the fastq file.
517 Filtered and trimmed reads were mapped to the *U. maydis* genome and its gene annotation
518 using STAR (version 2.5.1b, GitHub; Dobin, Davis et al., 2013), allowing up to two
519 mismatches and without soft-clipping on the 5′ end of the reads. Only uniquely mapped reads
520 were kept for further analysis.
521 After mapping and filtering, duplicate reads were marked using the *dedup* function from
522 bamUtil (version 1.0.7; https://github.com/statgen/bamUtil) and removed if carrying an
523 identical random barcode, and hence representing technical duplicates. The nucleotide
524 position upstream of each aligned read was considered as the 'crosslink nucleotide', with each
525 read counted as individual 'crosslink event'. The total number of crosslink events for the
526 different iCLIP libraries can be found in Fig. S3A. To assess the reproducibility between
527 biological replicates (Fig. S3C), we counted the number of crosslink events within each gene.
528 For the identification of putative RBP binding sites, peak calling was performed on
529 merged replicates for each RBP using ASPeak (Kucukural, Ozadam et al., 2013). The
530 predicted peaks were centred on the summit (i.e. the first position with highest number of
531 crosslink events within the peak) and then extended to 9-nt. Overlapping peaks were merged
532 and newly centred as described above. To account for reproducibility, we required each
533 binding site to be detected by at least 5 crosslink events from each biological replicate. We
534 further removed all Rrm4 and Grp1 binding sites that overlapped by at least 1 nt with any of
535 88 reproducible Gfp binding sites. This yielded a total of 14,120 binding site clusters sites for
536 Rrm4 and 18,155 binding sites for Grp1 (Fig. S3).
537 In order to facilitate comparisons between binding sites, crosslink events from both
538 replicates were summed up within each binding site and represented as 'signal-over-
539 background' (SOB). Background for each gene was the number of crosslink events outside

bioRxiv preprint doi: https://doi.org/10.1101/418079; this version posted September 14, 2018. The copyright holder for this preprint (which was not certified by peer review) is the author/funder, who has granted bioRxiv a license to display the preprint in perpetuity. It is made available under aCC-BY-NC-ND 4.0 International license.

the binding sites divided by the number of nucleotides in the gene that harbour such background crosslink events. Only binding sites associated with the top 25% of the SOB distribution for each RBP were taken into consideration for further analyses. This procedure yielded a total of 6,412 and 6,478 binding sites for Rrm4 and Grp1, respectively (Fig. 3B). The binding sites corresponded to 3,262 and 3,165 target transcripts for Rrm4 and Grp1, respectively. To define a high-confidence set of target genes that are exclusively bound by Rrm4 and show no evidence of Grp1 binding, we subtracted the full set of identified Grp1 binding sites (before SOB filtering), and vice versa. When assigning genomic nucleotides and RBP binding sites to distinct transcript regions (Fig. 3D), we applied the following hierarchy to resolve overlapping annotation: 3´ UTR > 5´ UTR > exon > intron.

Enriched sequence motifs around RBP binding sites were identified using DREME (Bailey, 2011; parameter –norc to search the coding strand only) to analyse a 30-nt window around all binding site summits compared to shuffled nucleotides. Based on the sequence profile and the UAUG content around binding sites (Fig. 5A-B), we counted a binding site as UAUG-containing if it harboured the motif with the last 5 nt of the 9-nt binding sites.

Analysing functional categories of cellular components on identified targets was performed using the FunCat annotation scheme (http://mips.gsf.de/funcatDB/; version 2.1, reference genome: p3_t237631_Ust_maydi_v2GB; Ruepp, Zollner et al., 2004). Categories were filtered during analysis for enrichment by setting the p-value threshold to <0.05.

RNASeq library preparation and data processing

RNA was extracted from AB33 hyphae 6 h.p.i. using the RNeasy Mini kit following the manufacturer's instructions for preparation of total RNA from yeast (Qiagen, Hilden, Germany). To this end, AB33 hyhae were opened in a Retsch ball mill (3 balls, d=4 mm ; MM400; Retsch, Haan, Germany) 4 times for 5 min at 30 Hz while keeping samples frozen

bioRxiv preprint doi: https://doi.org/10.1101/418079; this version posted September 14, 2018. The copyright holder for this preprint (which was not certified by peer review) is the author/funder, who has granted bioRxiv a license to display the preprint in perpetuity. It is made available under aCC-BY-NC-ND 4.0 International license.

using liquid nitrogen. The resulting cell powder was resolved in 450 µl RLT buffer (+β-mercapthoethanol) and centrifuged at 13,000 rpm for 2 min at 4°C. The supernatant was transferred to a new reaction tube, mixed with 1 volume 70% EtOH and then added to the RNeasy spin column. All following processing steps were performed according to manufacturer's instructions. TruSeq RNA Library Prep kit v2 (Illumina, San Diego, CA, USA) was used for cDNA library generation. The cDNA libraries were sequenced using the HiSeq 2000 platform (Illumina) with 151-nt single-end reads.

Basic quality checks were applied to all sequenced reads using FastQC (https://www.bioinformatics.babraham.ac.uk/projects/fastqc/). Afterwards, RNA-Seq reads were trimmed based on sequencing quality (Phred score) using Flexbar (version 3.0.3; Dodt et al., 2012). Specifically, adapter sequences were removed (TruSeq Universal Adapter), and reads were trimmed at the first position with a Phred score < 20 and removed if the remaining read length was less than 20 nt. The trimmed reads were mapped to the *U. maydis* genome and its gene annotation using STAR (version 2.5.3a; Dobin et al., 2013), allowing up to five mismatches with soft-clipping. Uniquely mapped reads were kept for further analysis.

Yeast three-hybrid analysis

Yeast three-hybrid experiments were performed as described previously (König et al., 2007, Vollmeister, Haag et al., 2009). To test the interaction with Rrm4, the plasmids encoding the RNA aptamers SELEX-A1(König et al., 2007) or mutated SELEX-A1 (mUAUG; this work) were cotransformed in strain L40 coat with the corresponding plasmids encoding for Rrm4 or mutated variants (König et al., 2007, SenGupta, Zhang et al., 1996). Transformed cells were incubated on SC -ura -leu plates (2-3 d at 28°C) before single clones were selected. Interaction was assayed as growth on selection medium SC -his +1 mM 3-AT (3-amino-1,2,4-triazole; Sigma-Aldrich) (3 d at 28°C). For the serial dilution assays, single clones were grown in SC -ura -leu medium to a starting OD_{600} = 0,5 and sequentially diluted 1:5 in water.

bioRxiv preprint doi: https://doi.org/10.1101/418079; this version posted September 14, 2018. The copyright holder for this preprint (which was not certified by peer review) is the author/funder, who has granted bioRxiv a license to display the preprint in perpetuity. It is made available under aCC-BY-NC-ND 4.0 International license.

The dilutions were then spotted on control (SC -ura -leu) and selection (SC -his +1 mM 3-AT) plates and incubated at 28°C.

Data accessibility

The iCLIP and RNASeq dataset are available from GEO under the accession numbers GSE109557 and GSE109560, respectively. The associated SuperSeries is GSE109561. The security token for anonymous Reviewer access to SuperSeries GSE109561 is gtabuyaihpatrix.

Acknowledgements

We thank Drs. J. Koepke and J. Kahnt for pilot Tap tag experiments and Dr T. Pohlmann for initial work on Grp1 fusion proteins. We acknowledge R. F. X. Sutandy for iCLIP support, M. Brüggemann for RNASeq data analysis, F. Finkernagel for bioinformatics and Dr. M. Seiler for critical reading of the manuscript. We are grateful to U. Gengenbacher and S. Esch for excellent technical assistance and members of the IMB Genomics core facility for technical assistance. The work was funded by grants from the Deutsche Forschungsgemeinschaft to MF (FE 448/8-1; FOR2333-TP03 FE-448/10-1; CEPLAS EXC1028) and KZ (FOR2333-TP10 ZA 881/1-1) and JK (SPP1935 KO 4566/2-1) and JU (European Research Council; 617837-Translate).

Competing interests

The authors declare that they have no competing interests.

bioRxiv preprint doi: https://doi.org/10.1101/418079; this version posted September 14, 2018. The copyright holder for this preprint (which was not certified by peer review) is the author/funder, who has granted bioRxiv a license to display the preprint in perpetuity. It is made available under aCC-BY-NC-ND 4.0 International license.

References

Bailey TL (2011) DREME: motif discovery in transcription factor ChIP-seq data. *Bioinformatics* 27: 1653-1659

Bastide A, Peretti D, Knight JR, Grosso S, Spriggs RV, Pichon X, Sbarrato T, Roobol A, Roobol J, Vito D, Bushell M, von der Haar T, Smales CM, Mallucci GR, Willis AE (2017) RTN3 is a novel cold-induced protein and mediates neuroprotective effects of RBM3. *Curr Biol* 27: 638-650

Baumann S, König J, Koepke J, Feldbrügge M (2014) Endosomal transport of septin mRNA and protein indicates local translation on endosomes and is required for correct septin filamentation. *EMBO Rep* 15: 94-102

Baumann S, Pohlmann T, Jungbluth M, Brachmann A, Feldbrügge M (2012) Kinesin-3 and dynein mediate microtubule-dependent co-transport of mRNPs and endosomes. *J Cell Sci* 125: 2740-2752

Baumann S, Takeshita N, Grün N, Fischer R, Feldbrügge M (2015) Live cell imaging of endosomal trafficking in fungi. In Methods in Mol Biol: Membrane trafficking, Tang BL (ed) pp 347-363. New York: Springer

Baumann S, Zander S, Weidtkamp-Peters S, Feldbrügge M (2016) Live cell imaging of septin dynamics in *Ustilago maydis*. In Septins, Gladfelter AS (ed) pp 143-149. Elsevier Inc.

Becht P, König J, Feldbrügge M (2006) The RNA-binding protein Rrm4 is essential for polarity in *Ustilago maydis* and shuttles along microtubules. *J Cell Sci* 119: 4964-4973

Becht P, Vollmeister E, Feldbrügge M (2005) Role for RNA-binding proteins implicated in pathogenic development of *Ustilago maydis*. *Euk Cell* 4: 121-133

Brachmann A, König J, Julius C, Feldbrügge M (2004) A reverse genetic approach for generating gene replacement mutants in *Ustilago maydis*. *Mol Gen Genom* 272: 216-226

Brachmann A, Weinzierl G, Kämper J, Kahmann R (2001) Identification of genes in the bW/bE regulatory cascade in *Ustilago maydis*. *Mol Microbiol* 42: 1047-1063

Cajigas IJ, Tushev G, Will TJ, tom Dieck S, Fuerst N, Schuman EM (2012) The local transcriptome in the synaptic neuropil revealed by deep sequencing and high-resolution imaging. *Neuron* 74: 453-466

Calabretta S, Richard S (2015) Emerging roles of disordered sequences in RNA-binding proteins. *Trends Biochem Sci* 40: 662-672

Campbell RE, Tour O, Palmer AE, Steinbach PA, Baird GS, Zacharias DA, Tsien RY (2002) A monomeric red fluorescent protein. *Proc Natl Acad Sci U S A* 99: 7877-7882

Chabanon H, Mickleburgh I, Burtle B, Pedder C, Hesketh J (2005) An AU-rich stem-loop structure is a critical feature of the perinuclear localization signal of c-myc mRNA. *Biochem J* 392: 475-483

Ciuzan O, Hancock J, Pamfil D, Wilson I, Ladomery M (2015) The evolutionarily conserved multifunctional glycine-rich RNA-binding proteins play key roles in development and stress adaptation. *Physiol Plant* 153: 1-11

Darnell JC, Van Driesche SJ, Zhang C, Hung KY, Mele A, Fraser CE, Stone EF, Chen C, Fak JJ, Chi SW, Licatalosi DD, Richter JD, Darnell RB (2011) FMRP stalls ribosomal translocation on mRNAs linked to synaptic function and autism. *Cell* 146: 247-261

Dobin A, Davis CA, Schlesinger F, Drenkow J, Zaleski C, Jha S, Batut P, Chaisson M, Gingeras TR (2013) STAR: ultrafast universal RNA-seq aligner. *Bioinformatics* 29: 15-21

Dodt M, Roehr JT, Ahmed R, Dieterich C (2012) FLEXBAR-flexible barcode and adapter processing for next-generation sequencing platforms. *Biology* 1: 895-905

Doyle M, Kiebler MA (2011) Mechanisms of dendritic mRNA transport and its role in synaptic tagging. *EMBO J* 30: 3540-3552

bioRxiv preprint doi: https://doi.org/10.1101/418079; this version posted September 14, 2018. The copyright holder for this preprint (which was not certified by peer review) is the author/funder, who has granted bioRxiv a license to display the preprint in perpetuity. It is made available under aCC-BY-NC-ND 4.0 International license.

Egan MJ, McClintock MA, Reck-Peterson SL (2012) Microtubule-based transport in filamentous fungi. *Curr Opin Microbiol* 15: 637-645

Eliscovich C, Singer RH (2017) RNP transport in cell biology: the long and winding road. *Current opinion in cell biology* 45: 38-46

Gehrke S, Wu Z, Klinkenberg M, Sun Y, Auburger G, Guo S, Lu B (2015) PINK1 and Parkin control localized translation of respiratory chain component mRNAs on mitochondria outer membrane. *Cell Metab* 21: 95-108

Gold VA, Chroscicki P, Bragoszewski P, Chacinska A (2017) Visualization of cytosolic ribosomes on the surface of mitochondria by electron cryo-tomography. *EMBO Rep* 18: 1786-1800

Goodrich JS, Clouse KN, Schupbach T (2004) Hrb27C, Sqd and Otu cooperatively regulate *gurken* RNA localization and mediate nurse cell chromosome dispersion in *Drosophila* oogenesis. *Development* 131: 1949-1958

Graber TE, Hebert-Seropian S, Khoutorsky A, David A, Yewdell JW, Lacaille JC, Sossin WS (2013) Reactivation of stalled polyribosomes in synaptic plasticity. *Proc Natl Acad Sci U S A* 110: 16205-16210

Guimaraes SC, Schuster M, Bielska E, Dagdas G, Kilaru S, Meadows BR, Schrader M, Steinberg G (2015) Peroxisomes, lipid droplets, and endoplasmic reticulum "hitchhike" on motile early endosomes. *J Cell Biol* 211: 945-954

Haag C, Pohlmann T, Feldbrugge M (2017) The ESCRT regulator Did2 maintains the balance between long-distance endosomal transport and endocytic trafficking. *PLoS Genet* 13: e1006734

Haag C, Steuten B, Feldbrügge M (2015) Membrane-coupled mRNA trafficking in fungi. *Annu Rev Microbiol* 69: 265-281

Halstead JM, Lionnet T, Wilbertz JH, Wippich F, Ephrussi A, Singer RH, Chao JA (2015) Translation. An RNA biosensor for imaging the first round of translation from single cells to living animals. *Science* 347: 1367-1671

Higuchi Y, Ashwin P, Roger Y, Steinberg G (2014) Early endosome motility spatially organizes polysome distribution. *J Cell Biol* 204: 343-357

Hogan DJ, Riordan DP, Gerber AP, Herschlag D, Brown PO (2008) Diverse RNA-binding proteins interact with functionally related sets of RNAs, suggesting an extensive regulatory system. *PLoS Biol* 6: e255

Holt CE, Bullock SL (2009) Subcellular mRNA localization in animal cells and why it matters. *Science* 326: 1212-1216

Huppertz I, Attig J, D'Ambrogio A, Easton LE, Sibley CR, Sugimoto Y, Tajnik M, König J, Ule J (2014) iCLIP: protein-RNA interactions at nucleotide resolution. *Methods* 65: 274-287

Huynh JR, Munro TP, Smith-Litiere K, Lepesant JA, St Johnston D (2004) The *Drosophila* hnRNPA/B homolog, Hrp48, is specifically required for a distinct step in osk mRNA localization. *Dev Cell* 6: 625-635

Imai K, Noda Y, Adachi H, Yoda K (2005) A novel endoplasmic reticulum membrane protein Rcr1 regulates chitin deposition in the cell wall of Saccharomyces cerevisiae. *J Biol Chem* 280: 8275-84

Jambor H, Surendranath V, Kalinka AT, Mejstrik P, Saalfeld S, Tomancak P (2015) Systematic imaging reveals features and changing localization of mRNAs in Drosophila development. *eLife* 4

Jung H, Yoon BC, Holt CE (2012) Axonal mRNA localization and local protein synthesis in nervous system assembly, maintenance and repair. *Nat Rev Neurosci* 13: 308-324

Kämper J, Kahmann R, Bölker M, Ma LJ, Brefort T, Saville BJ, Banuett F, Kronstad JW, Gold SE, Müller O, Perlin MH, Wösten HA, de Vries R, Ruiz-Herrera J, Reynaga-Pena CG, Snetselaar K, McCann M, Pérez-Martín J, Feldbrügge M, Basse CW et al. (2006)

bioRxiv preprint doi: https://doi.org/10.1101/418079; this version posted September 14, 2018. The copyright holder for this preprint (which was not certified by peer review) is the author/funder, who has granted bioRxiv a license to display the preprint in perpetuity. It is made available under aCC-BY-NC-ND 4.0 International license.

Insights from the genome of the biotrophic fungal plant pathogen *Ustilago maydis*. *Nature* 444: 97-101

Kang H, Park SJ, Kwak KJ (2013) Plant RNA chaperones in stress response. *Trends Plant Sci* 18: 100-106

Kato M, Han TW, Xie S, Shi K, Du X, Wu LC, Mirzaei H, Goldsmith EJ, Longgood J, Pei J, Grishin NV, Frantz DE, Schneider JW, Chen S, Li L, Sawaya MR, Eisenberg D, Tycko R, McKnight SL (2012) Cell-free formation of RNA granules: low complexity sequence domains form dynamic fibers within hydrogels. *Cell* 149: 753-767

Kim JS, Park SJ, Kwak KJ, Kim YO, Kim JY, Song J, Jang B, Jung CH, Kang H (2007) Cold shock domain proteins and glycine-rich RNA-binding proteins from *Arabidopsis thaliana* can promote the cold adaptation process in *Escherichia coli*. *Nucleic Acids Res* 35: 506-516

Koepke J, Kaffarnik F, Haag C, Zarnack K, Luscombe NM, König J, Ule J, Kellner R, Begerow D, Feldbrügge M (2011) The RNA-binding protein Rrm4 is essential for efficient secretion of endochitinase Cts1. *Mol Cell Proteom* 10: M111.011213 1-15

König J, Baumann S, Koepke J, Pohlmann T, Zarnack K, Feldbrügge M (2009) The fungal RNA-binding protein Rrm4 mediates long-distance transport of *ubi1* and *rho3* mRNAs. *EMBO J* 28: 1855-1866

König J, Julius C, Baumann S, Homann M, Göringer HU, Feldbrügge M (2007) Combining SELEX and yeast three-hybrid system for *in vivo* selection and classification of RNA aptamers. *RNA* 13: 614-622

König J, Zarnack K, Luscombe NM, Ule J (2012) Protein-RNA interactions: new genomic technologies and perspectives. *Nat Rev Genet* 13: 77-83

König J, Zarnack K, Rot G, Curk T, Kayikci M, Zupan B, Turner DJ, Luscombe NM, Ule J (2010) iCLIP reveals the function of hnRNP particles in splicing at individual nucleotide resolution. *Nat Struct Mol Biol* 17: 909-915

Kozak M (2005) Regulation of translation via mRNA structure in prokaryotes and eukaryotes. *Gene* 361: 13-37

Kucukural A, Ozadam H, Singh G, Moore MJ, Cenik C (2013) ASPeak: an abundance sensitive peak detection algorithm for RIP-Seq. *Bioinformatics* 29: 2485-2486

Larkin MA, Blackshields G, Brown NP, Chenna R, McGettigan PA, McWilliam H, Valentin F, Wallace IM, Wilm A, Lopez R, Thompson JD, Gibson TJ, Higgins DG (2007) Clustal W and Clustal X version 2.0. *Bioinformatics* 23: 2947-2948

Lécuyer E, Yoshida H, Parthasarathy N, Alm C, Babak T, Cerovina T, Hughes TR, Tomancak P, Krause HM (2007) Global analysis of mRNA localization reveals a prominent role in organizing cellular architecture and function. *Cell* 131: 174-187

Lesnik C, Golani-Armon A, Arava Y (2015) Localized translation near the mitochondrial outer membrane: An update. *RNA Biol* 12: 801-809

Levadoux M, Mahon C, Beattie JH, Wallace HM, Hesketh JE (1999) Nuclear import of metallothionein requires its mRNA to be associated with the perinuclear cytoskeleton. *The Journal of biological chemistry* 274: 34961-34966

Margeot A, Blugeon C, Sylvestre J, Vialette S, Jacq C, Corral-Debrinski M (2002) In *Saccharomyces cerevisiae*, *ATP2* mRNA sorting to the vicinity of mitochondria is essential for respiratory function. *EMBO J* 21: 6893-6904

Martin KC, Ephrussi A (2009) mRNA localization: gene expression in the spatial dimension. *Cell* 136: 719-730

Merzlyak EM, Goedhart J, Shcherbo D, Bulina ME, Shcheglov AS, Fradkov AF, Gaintzeva A, Lukyanov KA, Lukyanov S, Gadella TW, Chudakov DM (2007) Bright monomeric red fluorescent protein with an extended fluorescence lifetime. *Nature methods* 4: 555-557

bioRxiv preprint doi: https://doi.org/10.1101/418079; this version posted September 14, 2018. The copyright holder for this preprint (which was not certified by peer review) is the author/funder, who has granted bioRxiv a license to display the preprint in perpetuity. It is made available under aCC-BY-NC-ND 4.0 International license.

Meyer K, Koster T, Nolte C, Weinholdt C, Lewinski M, Grosse I, Staiger D (2017) Adaptation of iCLIP to plants determines the binding landscape of the clock-regulated RNA-binding protein AtGRP7. *Genome Biol* 18: 204

Mofatteh M, Bullock SL (2017) SnapShot: Subcellular mRNA localization. *Cell* 169: 178.e1

Peretti D, Bastide A, Radford H, Verity N, Molloy C, Martin MG, Moreno JA, Steinert JR, Smith T, Dinsdale D, Willis AE, Mallucci GR (2015) RBM3 mediates structural plasticity and protective effects of cooling in neurodegeneration. *Nature* 518: 236-239

Pohlmann T, Baumann S, Haag C, Albrecht M, Feldbrügge M (2015) A FYVE zinc finger domain protein specifically links mRNA transport to endosome trafficking. *eLife* 4: 10.7554/eLife.06041

Ram AF, Klis FM (2006) Identification of fungal cell wall mutants using susceptibility assays based on Calcofluor white and Congo red. *Nat Protoc* 1: 2253-2256

Rangaraju V, Tom Dieck S, Schuman EM (2017) Local translation in neuronal compartments: how local is local? *EMBO Rep* 18: 693-711

Rothbauer U, Zolghadr K, Muyldermans S, Schepers A, Cardoso MC, Leonhardt H (2008) A versatile nanotrap for biochemical and functional studies with fluorescent fusion proteins. *Mol Cell Proteomics* 7: 282-289

Ruepp A, Zollner A, Maier D, Albermann K, Hani J, Mokrejs M, Tetko I, Guldener U, Mannhaupt G, Münsterkötter M, Mewes HW (2004) The FunCat, a functional annotation scheme for systematic classification of proteins from whole genomes. *Nucleic Acids Res* 32: 5539-5545

Salogiannis J, Egan MJ, Reck-Peterson SL (2016) Peroxisomes move by hitchhiking on early endosomes using the novel linker protein PxdA. *The Journal of cell biology* 212: 289-296

Salogiannis J, Reck-Peterson SL (2016) Hitchhiking: a non-canonical mode of microtubule-based transport. *Trends in cell biology* 27: 141-150

Sen A, Cox RT (2016) Clueless is a conserved ribonucleoprotein that binds the ribosome at the mitochondrial outer membrane. *Biol Open* 5: 195-203

SenGupta DJ, Zhang B, Kraemer B, Pochart P, Fields S, Wickens M (1996) A three-hybrid system to detect RNA-protein interactions *in vivo*. *Proc Natl Acad Sci U S A* 93: 8496-8501

Shaner NC, Campbell RE, Steinbach PA, Giepmans BN, Palmer AE, Tsien RY (2004) Improved monomeric red, orange and yellow fluorescent proteins derived from *Discosoma* sp. red fluorescent protein. *Nat Biotechnol* 22: 1567-1572

Steinberg G (2014) Endocytosis and early endosome motility in filamentous fungi. *Curr Opin Microbiol* 20: 10-18

Straube A, Enard W, Berner A, Wedlich-Söldner R, Kahmann R, Steinberg G (2001) A split motor domain in a cytoplasmic dynein. *EMBO J* 20: 5091-5100

Van Nostrand EL, Pratt GA, Shishkin AA, Gelboin-Burkhart C, Fang MY, Sundararaman B, Blue SM, Nguyen TB, Surka C, Elkins K, Stanton R, Rigo F, Guttman M, Yeo GW (2016) Robust transcriptome-wide discovery of RNA-binding protein binding sites with enhanced CLIP (eCLIP). *Nature methods* 13: 508-514

Vollmeister E, Feldbrügge M (2010) Posttranscriptional control of growth and development in *Ustilago maydis*. *Curr Opin Microbio* 13: 693-699

Vollmeister E, Haag C, Zarnack K, Baumann S, König J, Mannhaupt G, Feldbrügge M (2009) Tandem KH domains of Khd4 recognize AUACCC and are essential for regulation of morphology as well as pathogenicity in *Ustilago maydis*. *RNA* 15: 2206-2218

Wu B, Eliscovich C, Yoon YJ, Singer RH (2016) Translation dynamics of single mRNAs in live cells and neurons. *Science* 352: 1430-1435

Yano T, Lopez de Quinto S, Matsui Y, Shevchenko A, Shevchenko A, Ephrussi A (2004) Hrp48, a *Drosophila* hnRNPA/B homolog, binds and regulates translation of oskar mRNA. *Dev Cell* 6: 637-648

bioRxiv preprint doi: https://doi.org/10.1101/418079; this version posted September 14, 2018. The copyright holder for this preprint (which was not certified by peer review) is the author/funder, who has granted bioRxiv a license to display the preprint in perpetuity. It is made available under aCC-BY-NC-ND 4.0 International license.

Ying Y, Wang XJ, Vuong CK, Lin CH, Damianov A, Black DL (2017) Splicing activation by Rbfox requires self-aggregation through Its tyrosine-rich domain. *Cell* 170: 312-323 e10

Zander S, Baumann S, Weidtkamp-Peters S, Feldbrügge M (2016) Endosomal assembly and transport of heteromeric septin complexes promote septin cytoskeleton formation. *J Cell Sci* 129: 2778-2792

Zarnegar BJ, Flynn RA, Shen Y, Do BT, Chang HY, Khavari PA (2016) irCLIP platform for efficient characterization of protein-RNA interactions. *Nature methods* 13: 489-492

Zhang Y, Chen Y, Gucek M, Xu H (2016) The mitochondrial outer membrane protein MDI promotes local protein synthesis and mtDNA replication. *EMBO J* 35: 1045-1057

Zhu X, Buhrer C, Wellmann S (2016) Cold-inducible proteins CIRP and RBM3, a unique couple with activities far beyond the cold. *Cellular and molecular life sciences : CMLS* 73: 3839-3859

bioRxiv preprint doi: https://doi.org/10.1101/418079; this version posted September 14, 2018. The copyright holder for this preprint (which was not certified by peer review) is the author/funder, who has granted bioRxiv a license to display the preprint in perpetuity. It is made available under aCC-BY-NC-ND 4.0 International license.

Figures

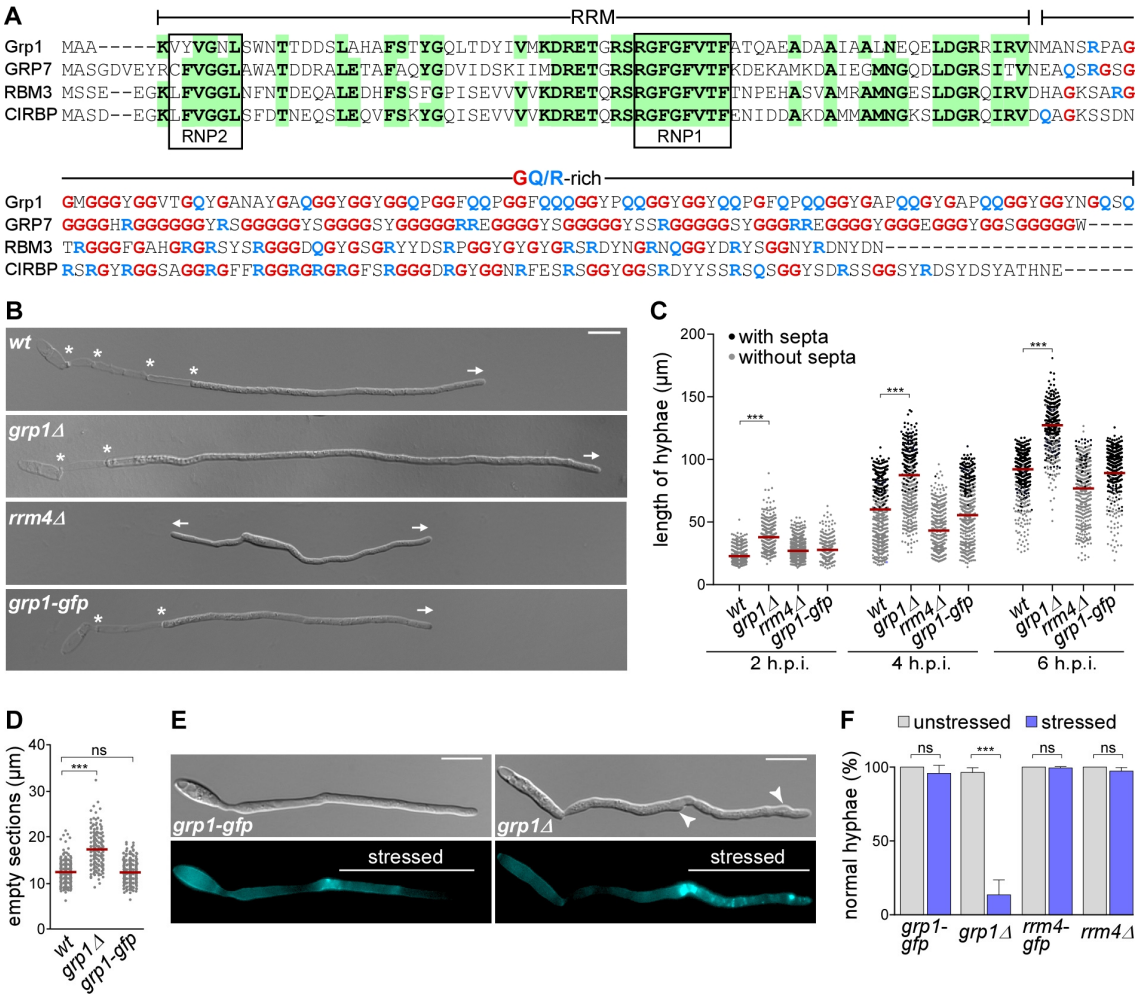

Fig. 1. Grp1 is important for hyphal growth under suboptimal conditions.
(**A**) Sequence alignment of glycine-rich proteins (Fig. S1B). *Um*Grp1 from *U. maydis* (UMAG_02412), *At*GRP7 (RBG7) from *A. thaliana* (NC_003071.7), *Hs*RBM3 and *Hs*CIRBP from *H. sapiens* (NC_000023.11 and NC_000019.10, respectively). Amino acid positions within RRM that are identical in at least three proteins are highlighted in green (boxes indicate RNA contact regions RNP1 and RNP2). Glycine and arginine/glutamine residues in the glycine-rich region are labelled in red and blue, respectively. (**B**) Hyphae of AB33 derivatives (6 h.p.i.). Growth direction and basal septa are marked by arrows and asterisks, respectively (size bar, 10 µm). (**C**) Hyphal length over time. Black and grey dots represent hyphae with and without septa, respectively (median, red line; ***, p value < 0.0001; Mann–Whitney U test). (**D**) Length of empty sections (see Fig. S1H); median, red line; n=3 independent experiments, > 100 hyphae analysed per experiment; ***, p value < 0.0001; ns, not significant, p value ≥ 0.05; Mann–Whitney U test). (**E**) Differential interference contrast (DIC, top) and fluorescence images (bottom) of AB33 hyphae (5 h.p.i.) stressed at 3 h.p.i. with cell wall inhibitor CFW (2.5 µM). Arrowheads indicate aberrant cell wall deformation (size bar, 10 µm). (**F**) Percentage of hyphae with normal cell walls with (stressed) and without (unstressed) CFW (mean of 3 independent experiments, > 100 hyphae analysed per experiment; error bars correspond to standard error of the mean, s.e.m.; ***, p value < 0.0001; ns, p value ≥ 0.05; unpaired Student's t-test).

bioRxiv preprint doi: https://doi.org/10.1101/418079; this version posted September 14, 2018. The copyright holder for this preprint (which was not certified by peer review) is the author/funder, who has granted bioRxiv a license to display the preprint in perpetuity. It is made available under aCC-BY-NC-ND 4.0 International license.

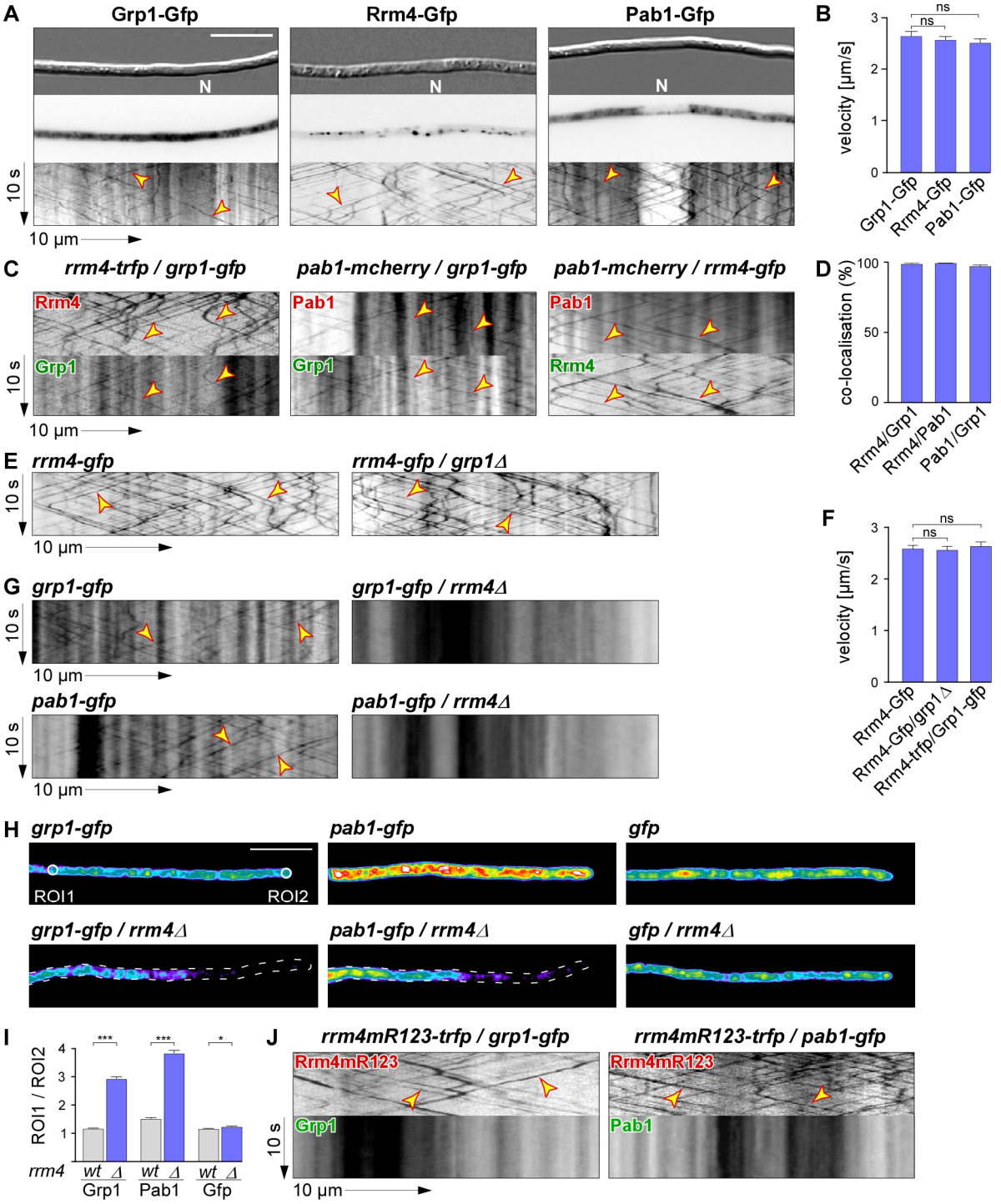

Fig. 2. Grp1 shuttles on Rrm4-positive endosomes throughout hyphae.

(**A**) Micrographs (DIC and inverted fluorescence image; size bar, 10 µm) and corresponding kymographs of AB33 hyphae (6 h.p.i.) expressing Grp1-Gfp, Rrm4-Gfp or Pab1-Gfp (arrow length on the left and bottom indicate time and distance, 10 s and 10 µm, respectively). Bidirectional movement is visible as diagonal lines (yellow arrowheads; N, nucleus; Supplemental Video 1). For an example image of a complete AB33 hypha, see Fig. S1A. (**B**) Bar diagram depicting velocity of fluorescent signals (velocity of tracks with > 5 µm processive movement; mean and error bars, s.e.m.; n=3 independent experiments, 11 hyphae analysed per experiment; ns, not significant, p value ≥ 0.05; unpaired Student's t-test). (**C**) Kymographs of hyphae of AB33 derivatives (6 h.p.i.) expressing pairs of red and green

bioRxiv preprint doi: https://doi.org/10.1101/418079; this version posted September 14, 2018. The copyright holder for this preprint (which was not certified by peer review) is the author/funder, who has granted bioRxiv a license to display the preprint in perpetuity. It is made available under aCC-BY-NC-ND 4.0 International license.

fluorescent proteins as indicated. Fluorescence signals were detected simultaneously using dual-view technology (arrow length as in A). Processive co-localising signals are marked by yellow arrowheads (Supplemental Videos 2-4). (**D**) Bar diagram depicting percentage of red fluorescent signals exhibiting co-localisation with the green fluorescent signal for strains shown in C (mean and error bars, s.e.m.; n=3 independent experiments, 11 hyphae each). (**E**) Kymographs comparing hyphae of AB33 derivatives (6 h.p.i.) expressing Rrm4-Gfp in the wild type (left) or *grp1Δ* strains (right) (processive signals marked by yellow arrowheads; arrow length on the left and bottom indicate time and distance, 10 s and 10 µm, respectively; Supplemental Video 5). (**F**) Velocity of fluorescent signals in kymographs of strains shown in E (velocity of tracks showing > 5 µm processive movement; mean and error bars, s.e.m.; n=3 independent experiments, at least 10 hyphae per experiment; ns, not significant, p value ≥ 0.05; unpaired Student's t-test). (**G**) Kymographs comparing hyphae (6 h.p.i.) expressing Grp1-Gfp or Pab1-Gfp in wild type (left) with *rrm4Δ* strains (right; processive signals marked by yellow arrowheads; arrow length as in A). (**H**) Hyphal tips (4 h.p.i.) of AB33 derivatives expressing Grp1-Gfp, Pab1-Gfp or Gfp alone comparing wild type (top) with *rrm4Δ* strains (bottom). Fluorescence micrographs in false colours (black/blue to red/white, low to high intensities, respectively; size bar, 10 µm; ROI1 and ROI2-labelled circles exemplarily indicate regions-of-interest analysed in E). **(I)** Ratio of signal intensities in strains showin in H comparing Gfp fluorescence at the tip (ROI1) and in close vicinity to the nucleus (ROI2) (see Materials and methods; mean and error bars, s.e.m.; more than 150 hyphae were analysed for each strain; *, p value < 0.01; ***, p value < 0.0001; Mann–Whitney U test). (**J**) Kymographs of hyphae of AB33 derivatives (6 h.p.i.) expressing pairs of red and green fluorescent proteins as indicated (arrow length as in A; Supplemental Videos 6-7). Fluorescence signals were detected simultaneously using dual-view technology. Processive co-localising signals are marked by yellow arrowheads. Note that processive movement is completely lost in the lower panels. Only static signals, visualised as vertical lines, are remaining.

bioRxiv preprint doi: https://doi.org/10.1101/418079; this version posted September 14, 2018. The copyright holder for this preprint (which was not certified by peer review) is the author/funder, who has granted bioRxiv a license to display the preprint in perpetuity. It is made available under aCC-BY-NC-ND 4.0 International license.

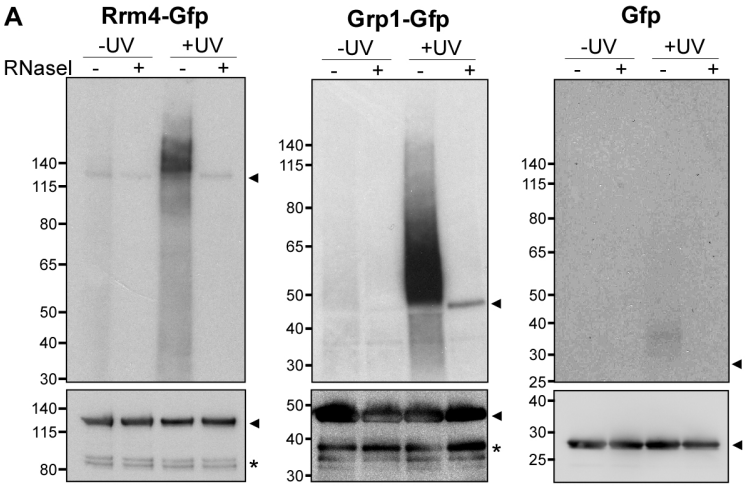

B

	Rrm4	Grp1
binding sites	6,412	6,478
target genes	3,262	3,165

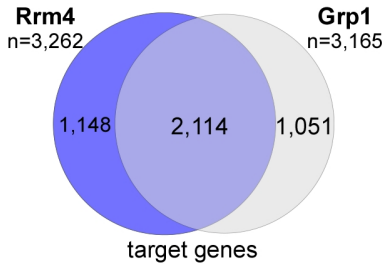

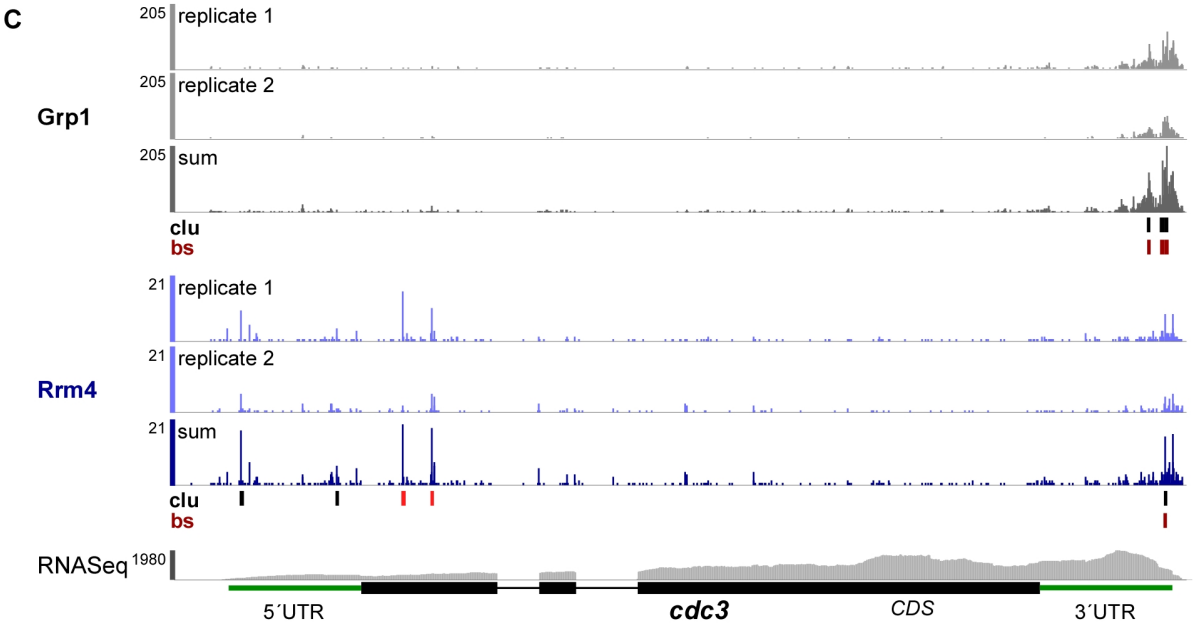

D

cellular compartment	Rrm4 & Grp1	Grp1
cytoplasm		
mitochondrion		
ER		
Golgi		
actin cytoskeleton		
transport vesicles		
plasma membrane		
mitochondrial matrix		
cytoskeleton		
adherence junction		
nucleus		
endosome		
cell junction		
vacuole		
mitochondrial IM		
chromosome		
centrosome		

not present

p value >0,01 <1e-02 <1e-04 <1e-06 <1e-08

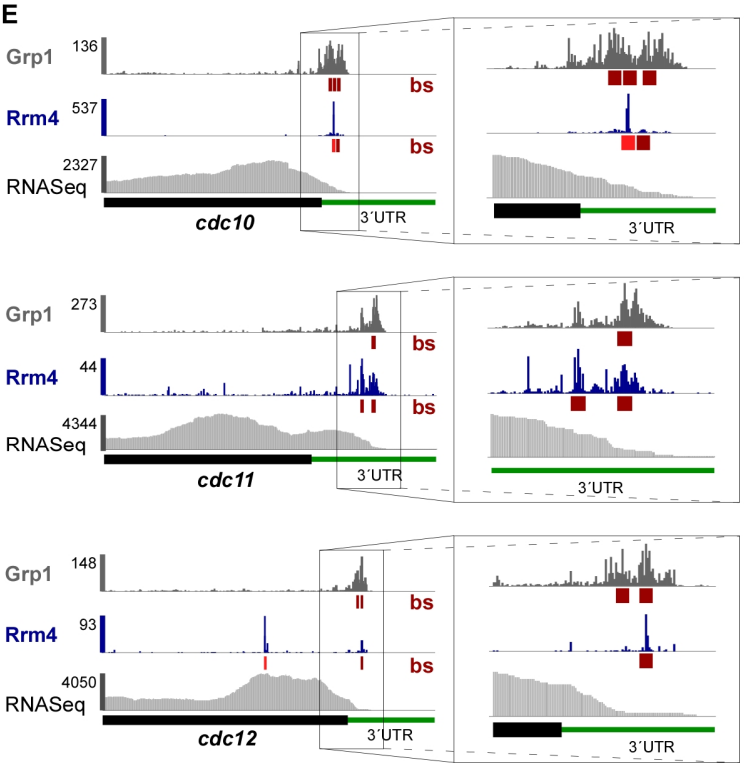

bioRxiv preprint doi: https://doi.org/10.1101/418079; this version posted September 14, 2018. The copyright holder for this preprint (which was not certified by peer review) is the author/funder, who has granted bioRxiv a license to display the preprint in perpetuity. It is made available under aCC-BY-NC-ND 4.0 International license.

Fig. 3. Rrm4 and Grp1 bind to thousands of target transcripts.

(**A**) Autoradiograph and Western blot analyses for representative iCLIP experiments with Rrm4-Gfp, Grp1-Gfp and Gfp. Upper part: Upon radioactive labelling of co-purified RNAs, the protein-RNA complexes were size-separated in a denaturing polyacrylamide gel. Protein-RNA complexes are visible as smear above the size of the protein (Rrm4-Gfp, 112 kDa; Grp1-Gfp, 45 kDa; Gfp, 27 kDa; indicated by arrowheads on the right). Samples with and without UV-C irradiation and RNase I (1/10 dilution) are shown. Lower part: corresponding Western blot analysis using α-Gfp antibody (arrowheads and asterisks indicate expected protein sizes and putative degradation products, respectively). (**B**) Summary of binding sites and target transcripts of Rrm4 and Grp1 (top). Venn diagram (below) illustrates the overlap of Rrm4 and Grp1 target transcripts. (**C**) iCLIP data for Rrm4 and Grp1 on *cdc3* (UMAG_10503; crosslink events per nucleotide from two experimental replicates [light grey/light blue] and merged data [grey/blue] from AB33 filaments, 6 h.p.i.). Tracks below the merged iCLIP data show clusters of crosslink events (clu, black; orange indicates overlap with UAUG) and filtered binding sites for each protein (bs, red; top 25% binding sites for Rrm4 and Grp1 based on 'signal-over-background'; see Materials and methods). RNASeq coverage from wild type AB33 filaments (6 h.p.i.) is shown for comparison. Gene model with exon/intron structure below was extended by 300 nt on either side to account for 5′ and 3′ UTRs (green). (**D**) Functional categories of cellular components (FunCat annotation scheme, Ruepp et al., 2004) for proteins encoded by target transcripts that are shared between Rrm4 and Grp1 (left) or unique to Grp1 (right). P values for the enrichment of the listed category terms are depicted by colour (see scale below). (**E**) iCLIP data (crosslink events from merged replicates) for Rrm4 (blue) and Grp1 (grey) as well as RNASeq coverage on selected target transcripts (*cdc10*, UMAG_10644; *cdc11*, UMAG_03449; *cdc12*, UMAG_03599). Enlarged regions (indicated by boxes) of the 3′ UTR (green) are shown on the right. Datasets and visualisation as in (C). Only filtered binding sites (bs) are shown (red; orange indicates overlap with UAUG).

bioRxiv preprint doi: https://doi.org/10.1101/418079; this version posted September 14, 2018. The copyright holder for this preprint (which was not certified by peer review) is the author/funder, who has granted bioRxiv a license to display the preprint in perpetuity. It is made available under aCC-BY-NC-ND 4.0 International license.

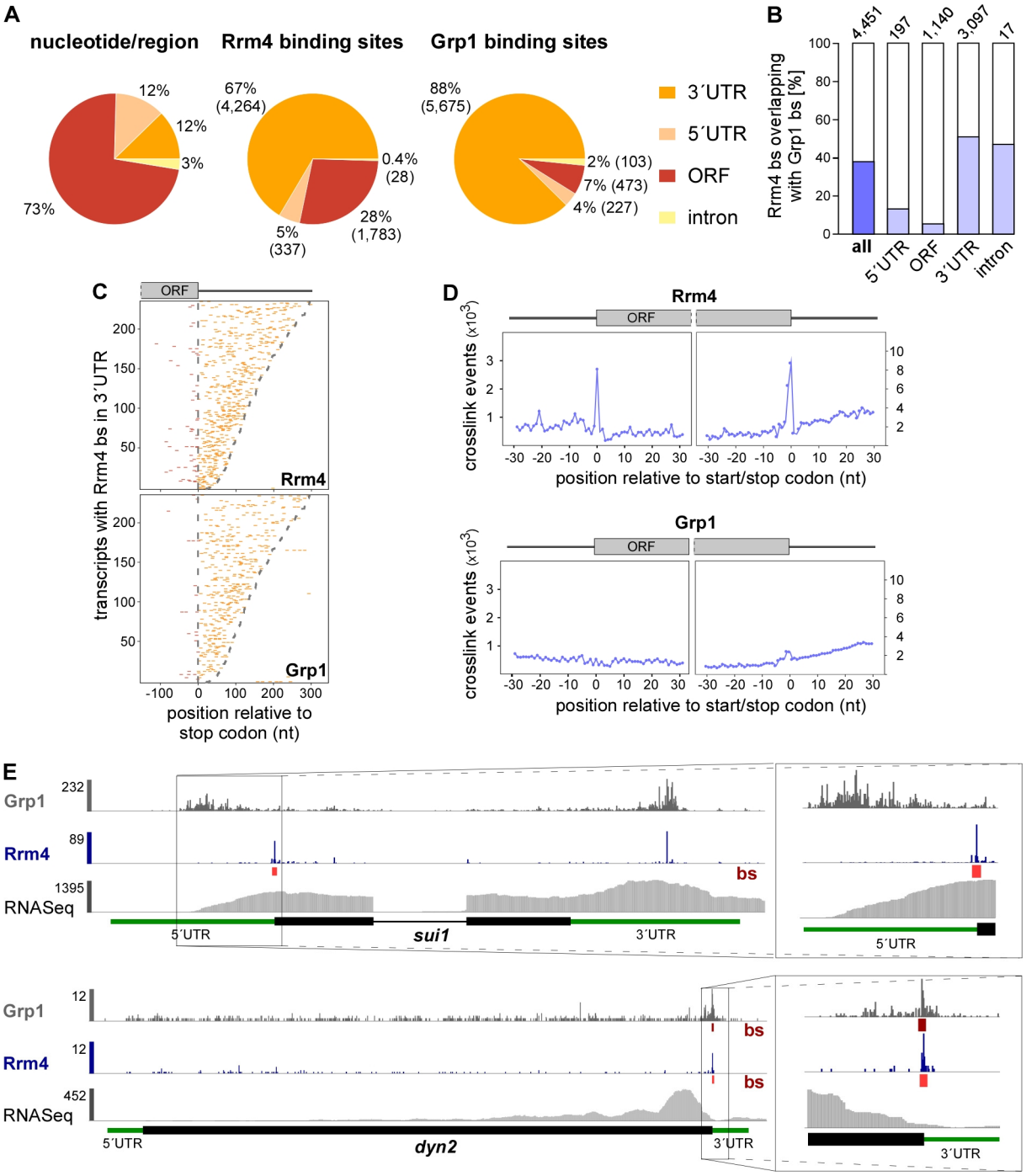

Fig. 4. Rrm4 binds target transcripts at the start and stop codon.

(**A**) Distribution of binding sites within different transcript regions: 5´ UTR, 3´ UTR, ORF and intron. Percentage and absolute number of binding sites are given for each category. On the left, a transcriptome-wide distribution of nucleotides per transcript region is shown for comparison. (**B**) Percentage of Rrm4 binding sites (bs) overlapping with Grp1 bs within shared target transcripts, shown for all bs and separated into transcript regions. The total number of binding sites per category is indicated on top. (**C**) Positional maps of Rrm4 (top) and Grp1 (bottom) bs relative to the stop codon (position 0). Binding sites in ORFs and 3´ UTR are given in red and orange, respectively. 234 target transcripts were randomly selected carrying an Rrm4 bs in the 3´ UTR (with > 100 Rrm4 crosslink events; out of 1,715 Rrm4/Grp1 shared targets with Rrm4 bs in 3´ UTR; Supplemental Table S6). (**D**) Metaprofiles of Rrm4 (top) and Grp1 (bottom) crosslink events relative to the start and stop codon

bioRxiv preprint doi: https://doi.org/10.1101/418079; this version posted September 14, 2018. The copyright holder for this preprint (which was not certified by peer review) is the author/funder, who has granted bioRxiv a license to display the preprint in perpetuity. It is made available under aCC-BY-NC-ND 4.0 International license.

(position 0). Note that crosslink events are substantially more frequent towards ORF ends, reflected in different y-axis scales. (**E**) Genome browser views of Rrm4 and Grp1 iCLIP events as well as RNASeq data of *sui1* (UMAG _02665) and *dyn2* (UMAG_04372). Visualisation as in Fig. 3C.

bioRxiv preprint doi: https://doi.org/10.1101/418079; this version posted September 14, 2018. The copyright holder for this preprint (which was not certified by peer review) is the author/funder, who has granted bioRxiv a license to display the preprint in perpetuity. It is made available under aCC-BY-NC-ND 4.0 International license.

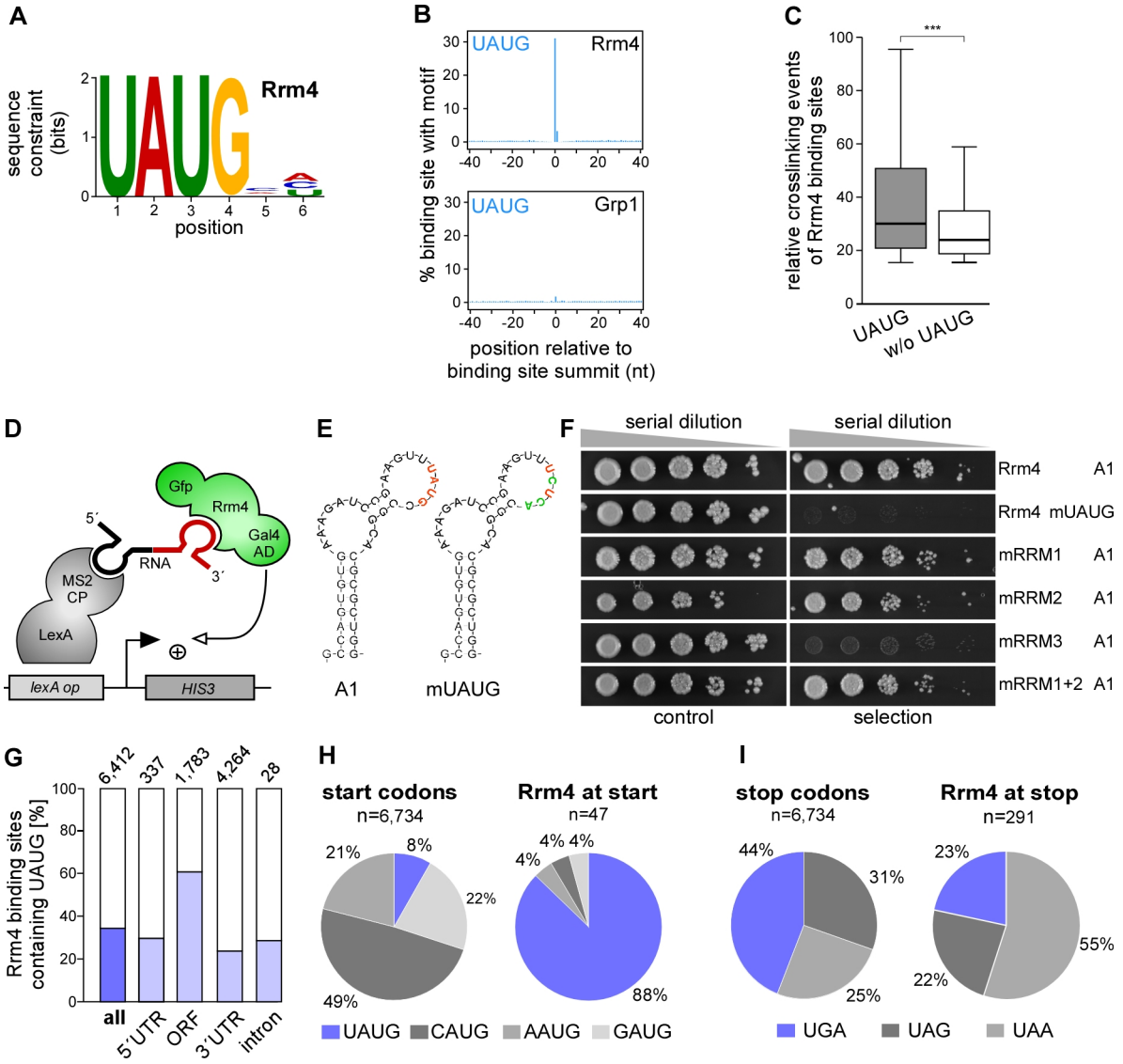

Fig. 5. Rrm4 recognises UAUG *in vivo*.

(**A**) Logo representation of the most enriched sequence motif at Rrm4 binding sites. At each position, the height of the stack is proportional to the information content, while the relative height of each nucleotide within the stack represents its relative frequency at this position. (**B**) Frequency of the Rrm4 motif UAUG around Rrm4 and Grp1 binding sites. Shown is the percentage of binding sites that harbour an UAUG starting at a given position in an 81-nt window around the binding site summit. (**C**) Box plot comparing relative crosslinking intensities (signal-over-background, SOB; see Materials and methods) of Rrm4 binding sites with or without UAUG (*** p value < 2.22e-16; unpaired Student's t-test). (**D**) Schematic representation of the yeast three-hybrid system: *lexA* operator (*lexA op*) sequences are bound by the LexA-MS2 coat protein (CP) hybrid (grey), recruiting the MS2-SELEX-RNA hybrid (black and red, respectively) to the promoter region of the *HIS3* reporter gene. Transcription is activated by binding of the third hybrid AD-Rrm4-Gfp (green) carrying a Gal4 activation domain (AD). (**E**) RNA structure prediction of aptamer SELEX-A1 with UAUG (red) or the mutated version mUAUG containing UCUC(A) (mutated bases in green). (**F**) Colony growth on control and selection plates of yeast cells expressing protein and RNA hybrids indicated on the right. RNA binding is scored by growth on selection plates (SC -his +3-AT, 3-amino-1,2,4-triazole). mRRMx, Rrm4 variants harbouring mutations in RRM1, 2, 3 or 1 and 2. (**G**)

bioRxiv preprint doi: https://doi.org/10.1101/418079; this version posted September 14, 2018. The copyright holder for this preprint (which was not certified by peer review) is the author/funder, who has granted bioRxiv a license to display the preprint in perpetuity. It is made available under aCC-BY-NC-ND 4.0 International license.

Percentage of Rrm4 bs containing the motif UAUG, shown for all bs and separated into transcript regions. Total number of binding sites is indicated on top. (**H**) Relative occurrence of NAUG sequence context for all (left) and Rrm4-bound (right) start codons. CAUG fits to the Kozak sequence in eukaryotes (Kozak, 2005). The fraction of UAUG coinciding with the Rrm4 recognition motif is shown in blue. This sequence context was strongly enriched among the Rrm4-bound target mRNAs, whereas it comprises only 8% of all annotated start codons in the *U. maydis* genome. (**I**) Relative contribution of the three stop codon variants to all (left) and Rrm4-bound stop codons (left). Although opal stop codons (UGA) fit best with a UAUG-containing binding site (UA<u>UGA</u>; present at 32 out of 63 bound UGA stop codons, 51%), they are depleted from Rrm4-bound stop codons.

bioRxiv preprint doi: https://doi.org/10.1101/418079; this version posted September 14, 2018. The copyright holder for this preprint (which was not certified by peer review) is the author/funder, who has granted bioRxiv a license to display the preprint in perpetuity. It is made available under aCC-BY-NC-ND 4.0 International license.

964

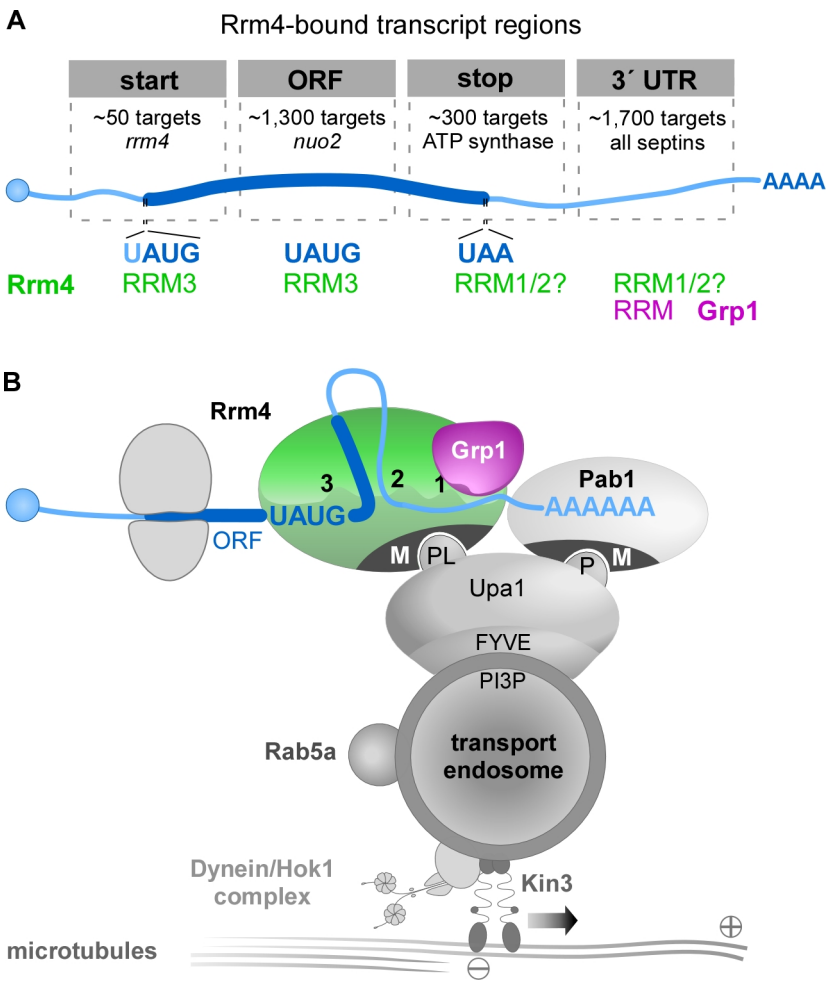

965 **Fig. 6. Model of Rrm4/Grp1-mediated endosomal mRNA transport**

966 (**A**) Schematic drawing of target transcript with Rrm4-bound regions on top (5´ cap structure,
967 blue circle; 5´ and 3´ UTR, light blue; ORF, dark blue; poly(A) tail, AAAA). Different
968 categories of Rrm4 target transcripts were defined according to the presence of Rrm4 binding
969 sites at the start codon, within the ORF, at the stop codon and in the 3´ UTR. Approximate
970 number of target transcripts and selected examples are given for each category. About 900 of
971 1,300 target transcripts with an Rrm4 binding site in the ORF harbour an UAUG motif within
972 the ORF binding site. Potential RRM domains of Rrm4 and Grp1 that may mediate RNA
973 binding in the different transcript regions are given in green and magenta, respectively. (**B**)
974 Model proposing the spatial arrangement of endosomal RBPs with bound target transcripts.
975 The three RRM domains of Rrm4 are schematically displayed and labelled by numbers
976 (FYVE zinc finger domain; PI3P, phosphatidylinositol 3-phosphate; M, MademoiseLLE
977 domain; P and PL, PAM2 and PAM2-like sequence, respectively; further details, see text).
978

bioRxiv preprint doi: https://doi.org/10.1101/418079; this version posted September 14, 2018. The copyright holder for this preprint (which was not certified by peer review) is the author/funder, who has granted bioRxiv a license to display the preprint in perpetuity. It is made available under aCC-BY-NC-ND 4.0 International license.

Supplemental Figures

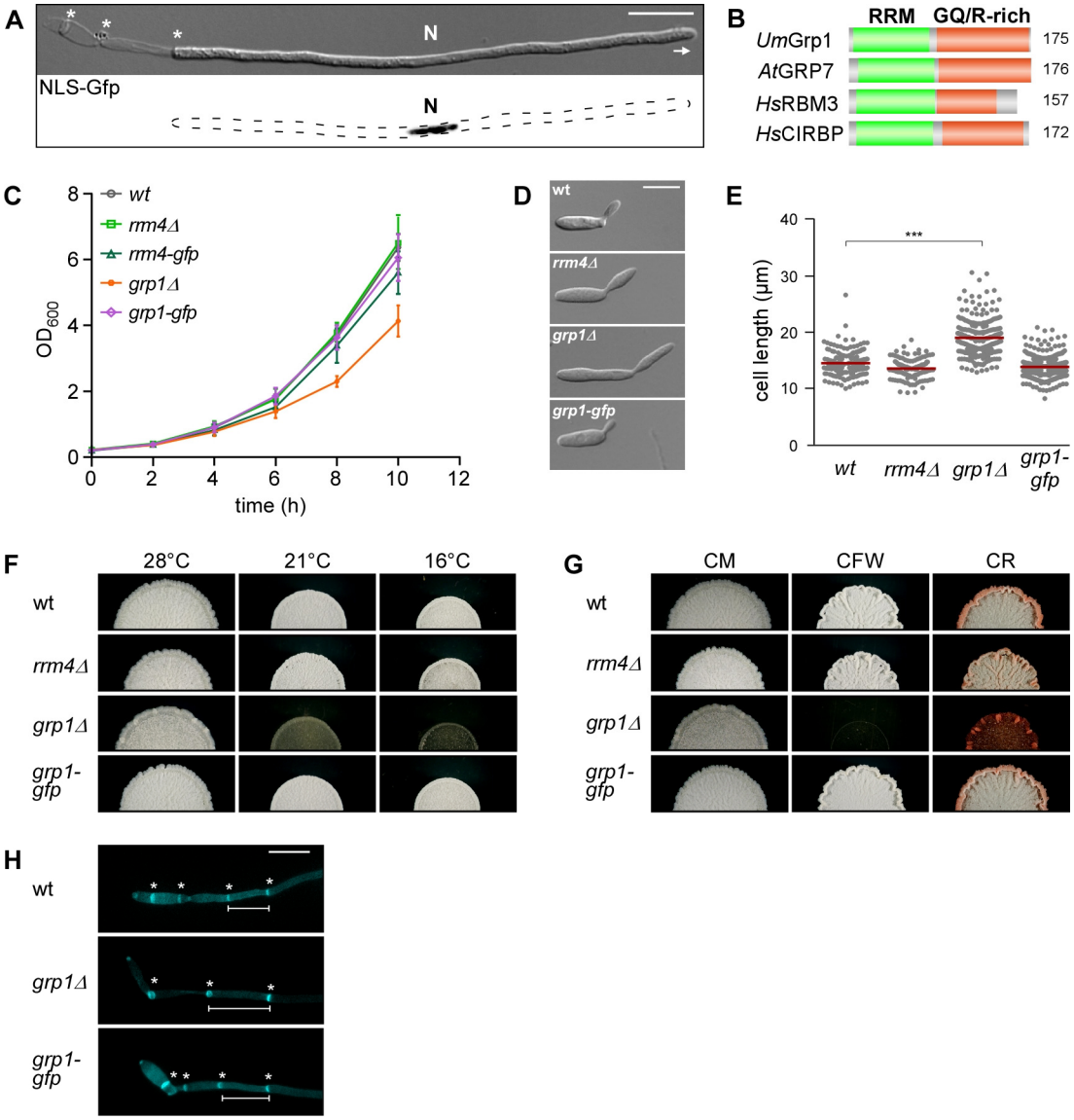

Fig. S1. Loss of Grp1 causes defects in cell growth.

(**A**) Hyphal form (6 hours post induction, h.p.i.) of laboratory strain AB33 expressing a Gfp-tagged protein with nuclear localisation signal to stain the nucleus (N; λN-NLS-Gfp, phage protein λN fused to triple Gfp, containing a nuclear localisation signal; inverted fluorescence image shown; size bar, 10 µm). Hyphae expand at the apical pole (arrow) and insert septa (asterisks) at the basal pole in regular time intervals resulting in the formation of empty sections. (**B**) Schematic representation of the domain architecture of four small glycine-rich proteins (RRM, RNA recognition motif, green; GQ/R, glycine-rich region with arginine or glutamine, red). *Um*Grp1 from *U. maydis* (UMAG_02412), *At*GRP7 from *Arabidopsis thaliana* (RBG7; NC_003071.7), *Hs*RBM3 and *Hs*CIRBP from *Homo sapiens* (NC_000023.11 and NC_000019.10, respectively). Number of amino acids indicated on the right. (**C**) Growth curve of indicated AB33 derivatives growing in liquid culture. (**D**) Differential interference contrast (DIC) images of AB33 derivatives as yeast-like budding cells (size bar, 10 µm). (**E**) Cell length of budding cells (median, red line; n=3 independent experiments, more than 40 cells per experiment; ***, p value < 0.0001; Mann–Whitney U test). (**F**) Colonies of indicated AB33 strains grown in the yeast form incubated at different

bioRxiv preprint doi: https://doi.org/10.1101/418079; this version posted September 14, 2018. The copyright holder for this preprint (which was not certified by peer review) is the author/funder, who has granted bioRxiv a license to display the preprint in perpetuity. It is made available under aCC-BY-NC-ND 4.0 International license.

temperatures (28°C for 1 d or 16°C and 21°C for 5 d). (**G**) Colonies of indicated AB33 strains grown in the yeast form. Incubated plates contained cell wall inhibitors (CM, complete medium for 1 d; CFW, 50 µM Calcofluor White for 4 d; CR, 57.4 µM Congo Red for 4 d). (**H**) Fluorescence images of the basal pole of hyphae of AB33 derivatives (6 h.p.i.). Septa (asterisks) were stained with CFW. White bars indicate exemplary length measurements of empty sections shown in Fig. 1D (size bar, 10 µm).

bioRxiv preprint doi: https://doi.org/10.1101/418079; this version posted September 14, 2018. The copyright holder for this preprint (which was not certified by peer review) is the author/funder, who has granted bioRxiv a license to display the preprint in perpetuity. It is made available under aCC-BY-NC-ND 4.0 International license.

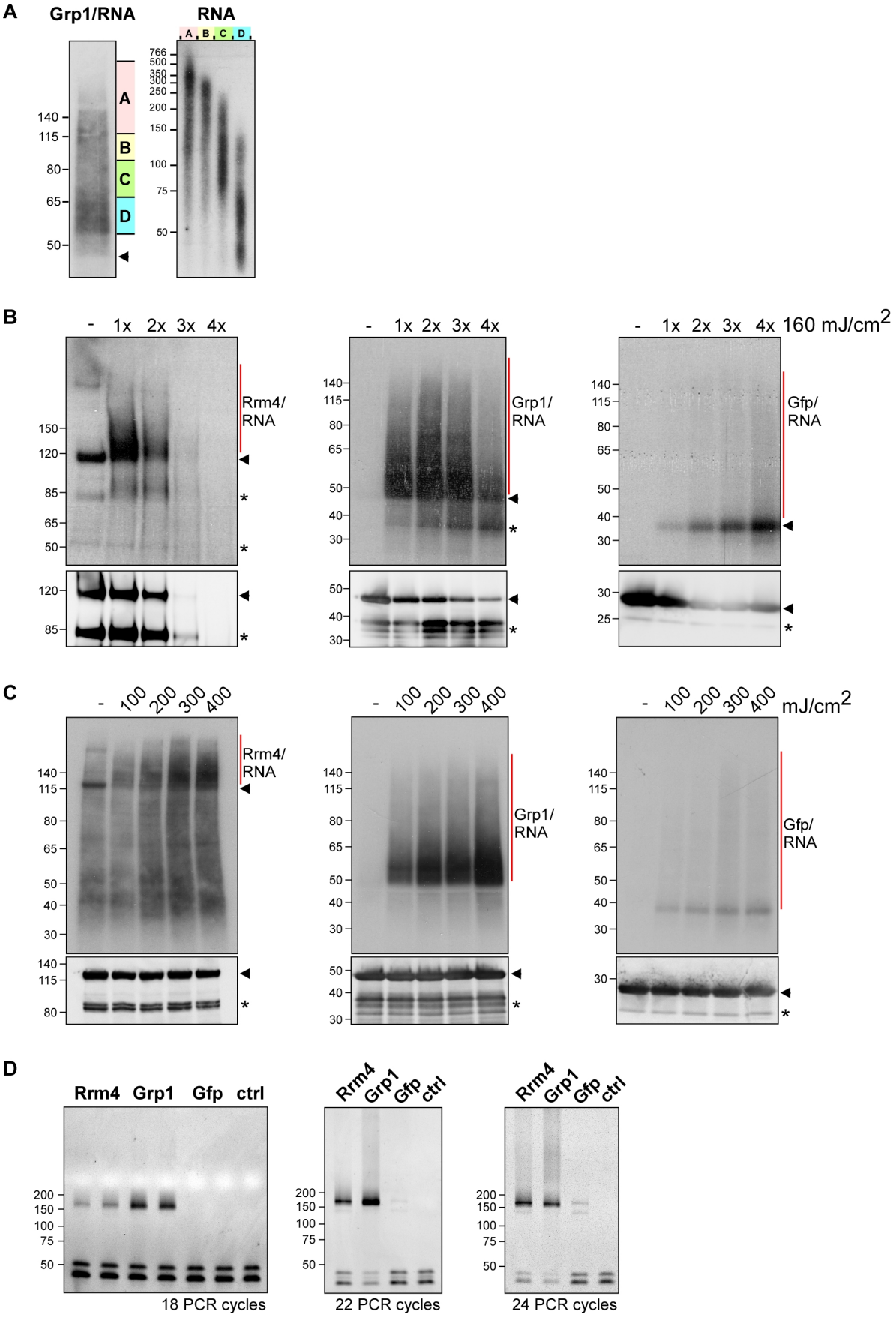

1004

bioRxiv preprint doi: https://doi.org/10.1101/418079; this version posted September 14, 2018. The copyright holder for this preprint (which was not certified by peer review) is the author/funder, who has granted bioRxiv a license to display the preprint in perpetuity. It is made available under aCC-BY-NC-ND 4.0 International license.

Fig. S2 Improving the iCLIP protocol for fungal RBPs.

(**A**) Grp1-Gfp/RNA complexes were size-separated on denaturing PAGE after UV-C irradiation and transferred to a nitrocellulose membrane (left). RNA was radioactively labelled, and protein-RNA complexes with covalently linked RNAs of different sizes were visible as smear above the expected molecular weight of the Grp1-Gfp protein (45 kDa; marked by arrowhead). RNA of four different regions of the membrane (A to D indicated on the right) were isolated from the membrane and size separated on a denaturing gel (6%) (right; nucleotide size marker on the left, bp). (**B**) Autoradiographs showing Rrm4-Gfp, Grp1-Gfp and Gfp in complex with RNA after UV-C irradiation at 0, 160, 320, 480 and 640 mJ/cm^2. Corresponding Western blots using anti-Gfp are shown below. Arrowheads indicate the expected molecular weight of the proteins (Rrm4-Gfp, 112 kDa; Grp1-Gfp, 45 kDa; Gfp, 27 kDa). After each irradiation step, the cells were mixed. Note that increased UV-C irradiation in combination with slow processing due to long time intervals was particularly harmful for the Rrm4 protein, which was completely degraded after four minutes of UV-C irradiation. (**C**) Autoradiographs showing Rrm4-Gfp, Grp1-Gfp and Gfp in complex with RNA after single UV-C irradiation at 0, 100, 200, 300 or 400 mJ/cm^2. This time, mixing breaks were omitted and cells were harvested as quickly as possible. Corresponding Western blots are shown below. Labelling as above. (**D**) Amplification of the Rrm4, Grp1 and Gfp derived cDNA libraries with different numbers of PCR cycles (between 18 and 24; ctrl, control without template cDNA). The PCR products were separated on a native gel (6%) and stained with SYBR green I (nucleotide size marker on the left, bp). The size of the cDNA insert together with the adapters (cDNA insert = 20-30 nt; L3 adapter, RT-primer and P3/P5 Solexa primers = 128 nt) is expected to be ~ 150-160 nt after amplification.

bioRxiv preprint doi: https://doi.org/10.1101/418079; this version posted September 14, 2018. The copyright holder for this preprint (which was not certified by peer review) is the author/funder, who has granted bioRxiv a license to display the preprint in perpetuity. It is made available under aCC-BY-NC-ND 4.0 International license.

A

		reads	uniquely mapped	crosslink events	Σ crosslink events	cluster of crosslinks	binding sites	genes
Rrm4	replicate1	14,791,625	9,027,052	2,777,064	4,683,060	14,120	6,412	3,262
	replicate2	24,757,620	16,269,064	1,905,996				
Grp1	replicate1	41,915,499	26,716,134	9,106,077	14,789,890	18,155	6,478	3,165
	replicate2	18,157,540	12,288,327	5,683,815				
Gfp	replicate1	671,922	208,847	73,398	153,851	88*	NA	59*
	replicate2	2,262,880	885,903	80,453				

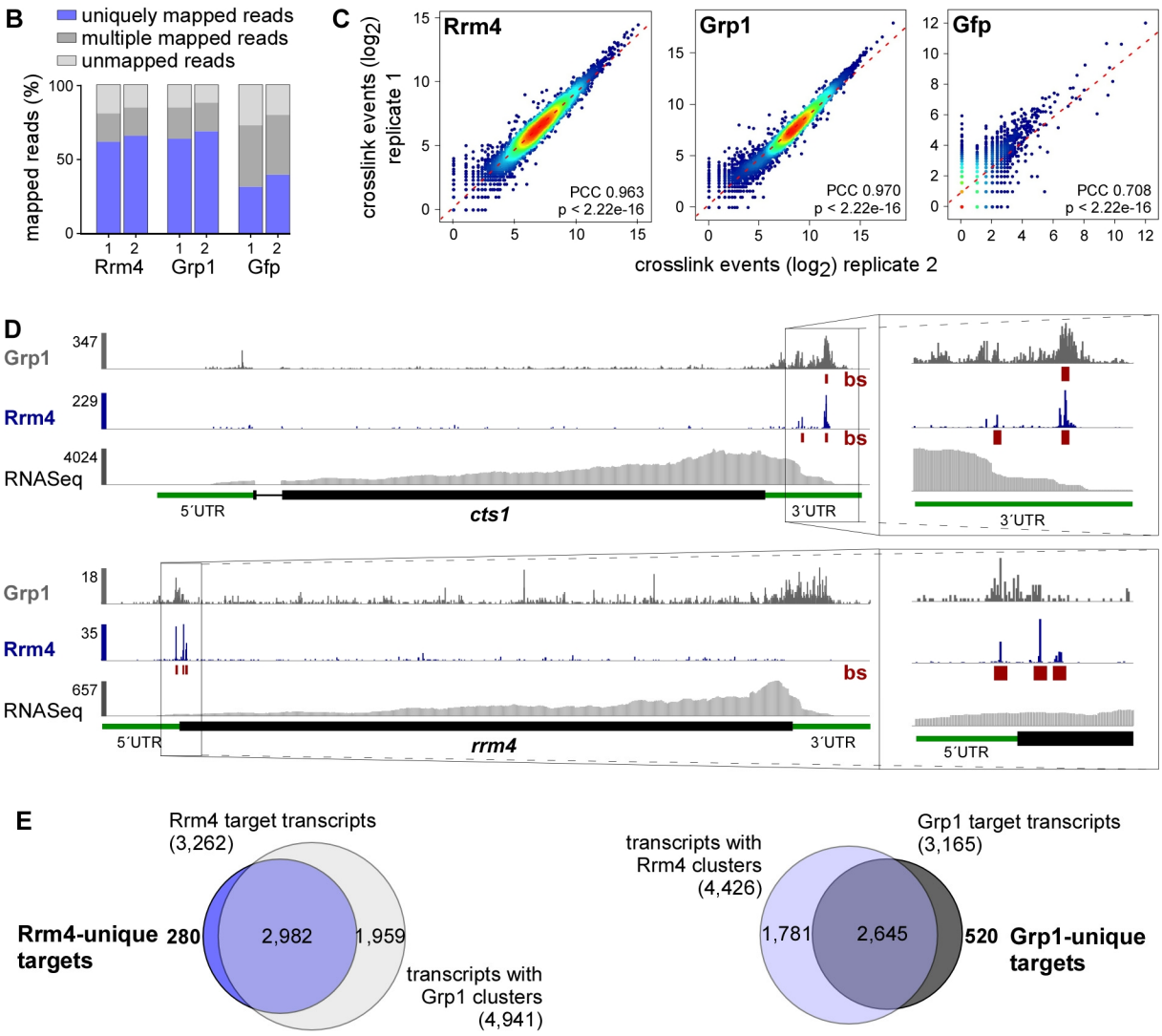

Fig. S3. Comparative iCLIP procedure results in high-quality dataset.

(**A**) Summary of the iCLIP libraries including initial number of sequencing reads, uniquely mapped reads, crosslink events (xlinks) for both replicates for Rrm4, Grp1 and Gfp. In addition, sum of crosslink events as well as resulting binding sites and target transcripts are given for merged replicates. *, Gfp binding sites were only filtered for reproducibility but not for relative signal intensity (SOB; see Material and methods). (**B**) Stacked bar chart showing percentage of reads mapping to a unique, multiple (multiple mapping) or no location (unmapped) in the *U. maydis* genome for Rrm4, Grp1 and Gfp. (**C**) Scatter plot comparing number of crosslink events per gene from two independent replicate experiments for Rrm4, Grp1 and Gfp (PCC, Pearson correlation coefficient). (**D**) Genome browser views of Rrm4 and Grp1 iCLIP events as well as RNASeq data of *cts1* (UMAG_10419) and *rrm4*

bioRxiv preprint doi: https://doi.org/10.1101/418079; this version posted September 14, 2018. The copyright holder for this preprint (which was not certified by peer review) is the author/funder, who has granted bioRxiv a license to display the preprint in perpetuity. It is made available under aCC-BY-NC-ND 4.0 International license.

(UMAG_10836). Visualisation as in Fig. 3C. (**E**) Venn diagram to identify target transcripts that are uniquely bound by Rrm4 (left) or Grp1 (right). Unique target transcripts (numbers given in bold) are selected only if they show no evidence of binding by the other RBP (considering all crosslink clusters, see Materials and methods).

bioRxiv preprint doi: https://doi.org/10.1101/418079; this version posted September 14, 2018. The copyright holder for this preprint (which was not certified by peer review) is the author/funder, who has granted bioRxiv a license to display the preprint in perpetuity. It is made available under aCC-BY-NC-ND 4.0 International license.

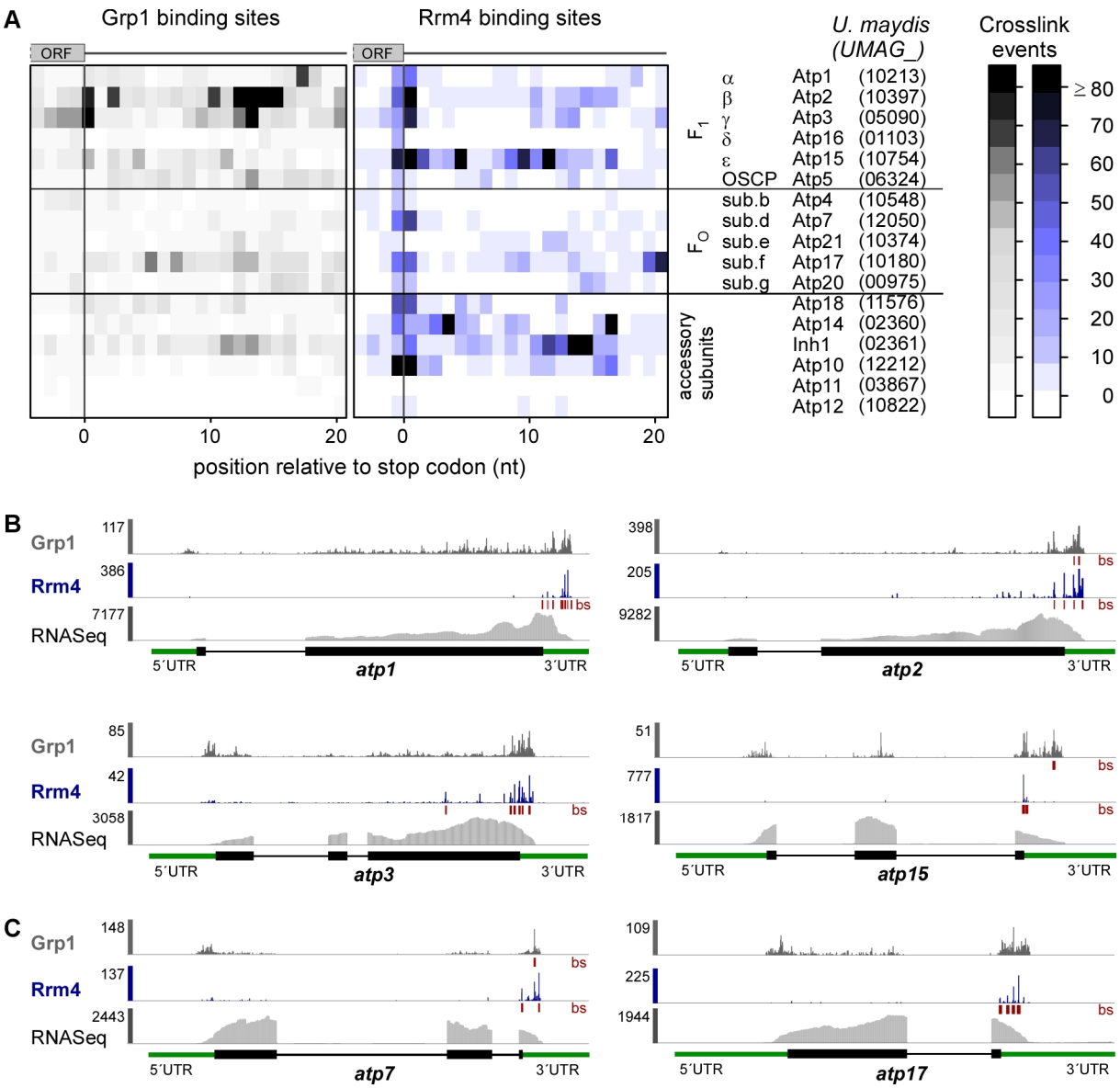

Fig. S4. Accumulation of crosslink events at stop codons of mRNAs encoding subunits of the mitochondrial F_OF_1-ATPase.

(**A**) Heatmap of crosslink events of Grp1 (left) and Rrm4 (right) in a window around the stop codons (position 0 = first position of 3´ UTR) of mRNAs encoding subunits of the mitochondrial F_OF_1-ATPase (nomenclature and gene identifiers for *U. maydis* on the right). Crosslink events per nucleotide are represented by a colour scale (right). (**B,C**) iCLIP data of Rrm4 and Grp1 as well as RNASeq data across selected mRNAs of the F_1 subcomplex (**B**) and F_O subcomplex (**C**) that carry an Rrm4 binding site precisely at the stop codon. Visualisation as in Fig. 3C.

bioRxiv preprint doi: https://doi.org/10.1101/418079; this version posted September 14, 2018. The copyright holder for this preprint (which was not certified by peer review) is the author/funder, who has granted bioRxiv a license to display the preprint in perpetuity. It is made available under aCC-BY-NC-ND 4.0 International license.

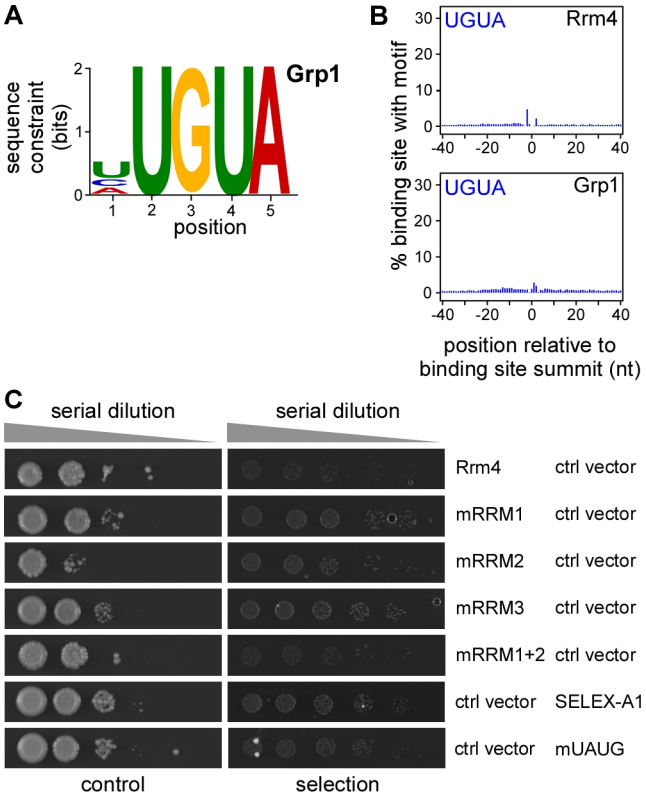

Fig. S5. Control experiments for the yeast three-hybrid analysis.

(**A**) Logo representation of the most enriched sequence motif at Grp1 binding sites. At each position, the height of the stack is proportional to the information content, while the relative height of each nucleotide within the stack represents its relative frequency at this position. (**B**) Frequency of UGUA around Rrm4 and Grp1 binding sites. Shown is the percentage of binding sites that harbour an UGUA starting at a given position in an 81-nt window around the binding site summit. Representation as in Fig. 5B. (**C**) Colony growth on control and selection plates of yeast cells expressing protein and RNA hybrids indicated on the right. RNA binding is scored by growth on selection plates (SC –his +3-AT, 3-amino-1,2,4-triazole). This control experiment demonstrates that growth on selection plates (see Fig. 5F) depends the presence of Rrm4 variant and cognate hybrid RNA. mRRMx, Rrm4 variants harbouring mutations in RRM 1, 2, 3 or 1 and 2.

bioRxiv preprint doi: https://doi.org/10.1101/418079; this version posted September 14, 2018. The copyright holder for this preprint (which was not certified by peer review) is the author/funder, who has granted bioRxiv a license to display the preprint in perpetuity. It is made available under aCC-BY-NC-ND 4.0 International license.

Supplemental Tables

Supplemental Table S1: Shared target transcripts that are bound by Rrm4 and Grp1. List of 2,114 target transcripts that harbour at least one binding site of Rrm4 and Grp1 as shown in Fig. 3B. Binding sites were assigned to distinct transcript regions, applying the following hierarchy to resolve overlapping annotation: 3′ UTR > 5′ UTR > exon > intron.

Supplemental Table S2: Grp1-unique target transcripts that are only bound by Grp1. List of 520 target transcripts that harbour at least one Grp1 binding site, but no Rrm4 binding site (subtracting the full set of unfiltered Rrm4 crosslink clusters as shown in Fig. S3E; see Materials and methods). Binding sites were assigned to distinct transcript regions, applying the following hierarchy to resolve overlapping annotation: 3′ UTR > 5′ UTR > exon > intron.

Supplemental Table S3: Rrm4-unique targets that are only bound by Rrm4. List of 280 target transcripts that harbour at least one Rrm4 binding site, but no Grp1 binding site (subtracting the full set of Grp1 crosslink clusters as shown in Fig. S3E; see Materials and methods). Binding sites were assigned to distinct transcript regions, applying the following hierarchy to resolve overlapping annotation: 3′ UTR > 5′ UTR > exon > intron.

Supplemental Table S4: Target transcripts with an Rrm4 binding site at the start codon. List of 47 target transcripts that harbour an Rrm4 binding site precisely overlapping the start codon. The NAUG sequence context is given for each Rrm4-bound start codon (as shown in Fig. 5H). CAUG fits to the Kozak sequence in eukaryotes, while UAUG represents the Rrm4 recognition motif.

Supplemental Table S5: Target transcripts with an Rrm4 binding site at the stop codon. List of 291 target transcripts that harbour an Rrm4 binding site precisely overlapping the stop

bioRxiv preprint doi: https://doi.org/10.1101/418079; this version posted September 14, 2018. The copyright holder for this preprint (which was not certified by peer review) is the author/funder, who has granted bioRxiv a license to display the preprint in perpetuity. It is made available under aCC-BY-NC-ND 4.0 International license.

codon. For each transcript, the type of stop codon is given. Rrm4 predominantly binds to UAA stop codons (as shown in Fig. 5I).

Supplemental Table S6: Selected target transcripts with Rrm4 binding sites in the 3´ UTR that are shown in Fig. 4C. For the positional maps in Fig. 4C, 234 target transcripts were randomly selected carrying an Rrm4 binding site in the 3´ UTR (with > 100 Rrm4 crosslink events; out of 1,715 Rrm4/Grp1 shared targets with Rrm4 binding site in 3´ UTR; Supplemental Table S1). For each target transcript, UMAG identifier, functional description and genomic coordinates of the annotated ORF are given together with the genomic coordinate of the manually annotated end position of the 3´ UTR (according to RNASeq coverage; see Materials and methods).

Supplemental Table S7: *U. maydis* strains used in this study. eGfp, enhanced Gfp. UMa, internal reference number.

Supplemental Table S8: *U. maydis* strains generated in this study. UMa and pUMa, internal reference numbers for strains and plasmids, respectively.

Supplemental Table S9: Plasmids generated in this study for *U. maydis*. pUMa, internal plasmid reference number.

Supplemental Table S10: Plasmids used for yeast three-hybrid system. pUMa, internal plasmid reference number.

bioRxiv preprint doi: https://doi.org/10.1101/418079; this version posted September 14, 2018. The copyright holder for this preprint (which was not certified by peer review) is the author/funder, who has granted bioRxiv a license to display the preprint in perpetuity. It is made available under aCC-BY-NC-ND 4.0 International license.

Legends to Supplemental Videos

Supplemental Video 1

Grp1-Gfp shuttles like Rrm4- and Pab1-positive endosomes in hyphae (central part shown, hyphal tip towards the right; N, nucleus; scale bar, 10 µm; timescale in seconds, 150 ms exposure time, 150 frames, 6 frames/s display rate, MPEG-4 format, 1660 kB; corresponds to Fig. 2A).

Supplemental Video 2

Processive Grp1-Gfp signals co-migrate with Rrm4-tRfp in hyphae (central part shown, hyphal tip towards the right; scale bar, 10 µm; timescale in seconds, 150 ms exposure time, 67 frames, 6 frames/s display rate; MPEG-4 format, 738 kB; corresponds to Fig. 2C).

Supplemental Video 3

Processive Grp1-Gfp signals co-migrate with Pab1-mCherry in hyphae (central part shown, hyphal tip towards the right; scale bar, 10 µm; timescale in seconds, 150 ms exposure time, 67 frames, x6 frames/s display rate; MPEG-4 format, 657 kB; corresponds to Fig. 2C).

Supplemental Video 4

Processive Rrm4-Gfp signals co-migrate with Pab1-mCherry in hyphae (central part shown, hyphal tip towards the right; scale bar, 10 µm; timescale in seconds, 150 ms exposure time, 67 frames, 6 frames/s display rate; MPEG-4 format, 738 kB; corresponds to Fig. 2C).

Supplemental Video 5

Shuttling of Rrm4 is independent of Grp1 (wild type hypha top, *grp1Δ* hypha bottom; scale bar, 10 µm; timescale in seconds,150 ms exposure time, 67 frames, 6 frames/s display rate; MPEG-4 format, 580 kB; corresponds to Fig. 3A).

Supplemental Video 6

Shuttling of Grp1-Gfp depends on RNA binding capacity of Rrm4 (hypha expressing Rrm4mR123-tRfp, with point mutations in RRM domains 1, 2 and 3 as well as Grp1-Gfp, top

bioRxiv preprint doi: https://doi.org/10.1101/418079; this version posted September 14, 2018. The copyright holder for this preprint (which was not certified by peer review) is the author/funder, who has granted bioRxiv a license to display the preprint in perpetuity. It is made available under aCC-BY-NC-ND 4.0 International license.

and bottom, respectively; scale bar, 10 µm; timescale in seconds, 150 ms exposure time, 67 frames, 6 frames/s display rate; MPEG-4 format, 1086 kB; corresponds to Fig. 3F).

Supplemental Video 7

Shuttling of Pab1-Gfp depends on RNA binding capacity of Rrm4 (hypha expressing Rrm4mR123-tRfp, with point mutations in RRM domains 1, 2 and 3 as well as Pab1-Gfp, top and bottom, respectively; scale bar, 10 µm; timescale in seconds, 150 ms exposure time, 67 frames, 6 frames/s display rate; MPEG-4 format, 1305 kB; corresponds to Fig. 3F).